Perspectives in Structural Chemistry

JEREMY K. BURDETT

Department of Chemistry, The University of Chicago, Chicago, Illinois 60637

Received May 4, 1987 (Revised Manuscript Received June 22, 1987)

Contents

Jeremy Burdett was born in England and educated at The Universities of Cambridge and Michigan. Since 1978 he has been on the faculty of The University of Chicago. He is presently Professor in The Department of Chemistry and in The James Franck Institute. His interests center around structural chemistry and the geometrical–electronic control of properties and reactivity.

I. Scope

The breadth of the area occupied by the structural chemistry of solids is enormous. Today chemists not only study the structure and properties of solids but also investigate reactions which occur in this state. These may be chemical in the usual sense in that a new species is generated, either photochemically or thermally, or they may best be described as phase transformations induced by pressure or temperature. The field of surface science is an ever-growing one and uses many of the concepts originally devized for systems with full three-dimensional periodicity. Solid-state chemistry encompasses, too, areas of organic, inorganic, and organometallic chemistry. We will see that some of the results of studies of the crystalline state have immediate application to the reactions of molecules in solution. Similarly, many of the ideas of use in the molecular area are of direct utility in solids. This article, introductory to those that follow in this issue, restricts itself to but a small corner of this area. It gives a personal view as to some important structural features of solids and how we may make progress in understanding the rapidly expanding collection of observations concerning them. The theory behind some of these structural problems follows from well-known ideas developed for the molecular area, but that associated with extended arrays often needs to make use of the techniques of tight-binding theory.[1] Many other problems are at present too difficult for us to approach in traditional theoretical ways and call upon other less conventional methods for their illumination. The diversity of problems we will mention is interesting in itself and is indicative of the richness of this field.

The layout of this article features three parts. The first highlights some structural features of solids and their geometrical description. In the second part we describe some simple but powerful models which have proven useful in the study of mainly continuous systems. Finally we apply the techniques of tight-binding theory to a selection of structural solid-state questions which have been mentioned earlier.

II. Structures of Solids

A. Solids and Molecules

Organic and inorganic chemists use structural data in two basic ways, one largely qualitative and the other more quantitative. With the increasing availability of automated diffractometers and structure-solving packages, the use of X-ray crystallography as a characterization tool is now routine in many laboratories. Thus the products of a reaction are often examined crystallographically as a matter of course. The immediate use of the results lies in the generation of a quick sketch of the molecule with its salient structural features, the bonds, or close interatomic contacts, emphasized. This process is in general much more difficult for materials based on extended arrays. The effort expended in finding a good single crystal is often the rate-determining step for the mineralogist, and synthetic strategies employed by the solid-state chemist are still in their infancy. However, once the crystal structure has been solved, a relationship may be sought between the crude collection of (x, y, z) coordinates and a geometrical model which will be useful in its description. This is invariably easier in "molecular" crystals, where a chemical unit is easily identified, than in the area of extended arrays. How the problem is tackled actually influences quite strongly the way we eventually ap-

0009-2665/88/0788-0003$06.50/0

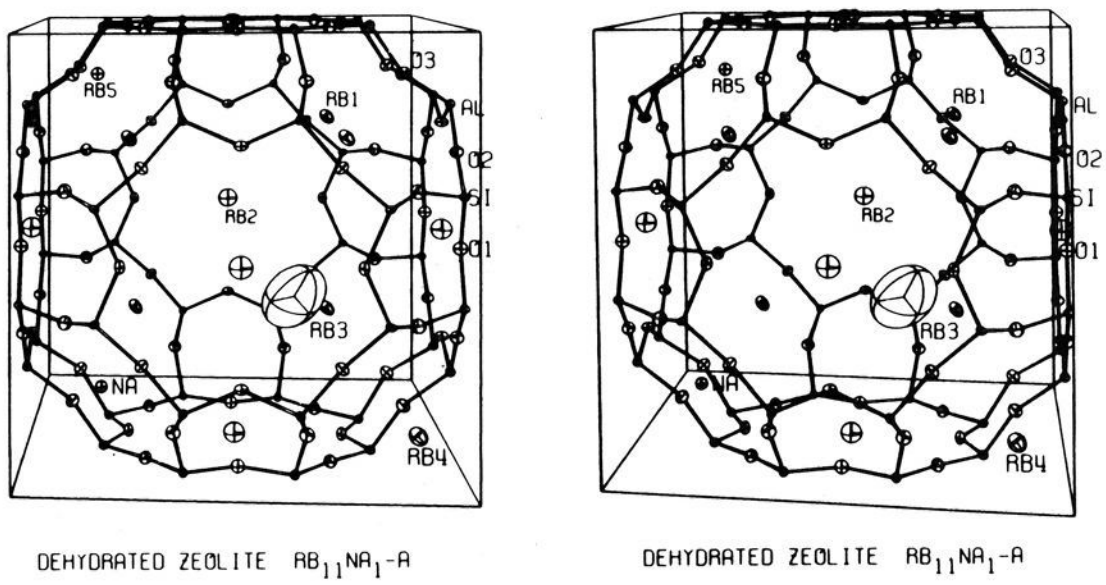

Figure 1. Supposedly "zero-coordinate" Rb^+ in a zeolite. Reprinted with permission from ref 15. Copyright 1978 Harper and Row.

proach the structural problem theoretically. "Billiard ball" models have usually engendered "ionic" theories, whereas the observation of some directional features in a structure, or the clear dependences of structure on electron count, has required the use of "covalent" models.[2]

In our dealings with solids we often make connections, both geometry and electronic, with molecules or molecular crystals. The molecules adamantane, and hexamethylenetetramine ($C_6H_{12}N_4$), **1**, have obvious

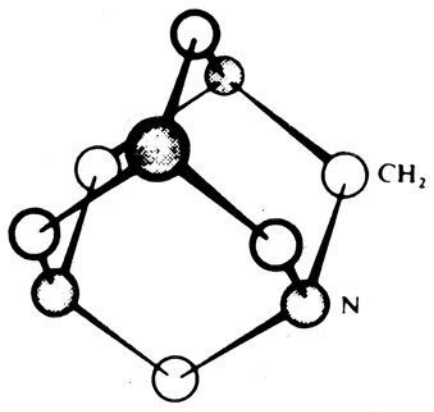

1

connections with the geometry found for crystalline cubic diamond, **2**. **1** is of particular interest since it

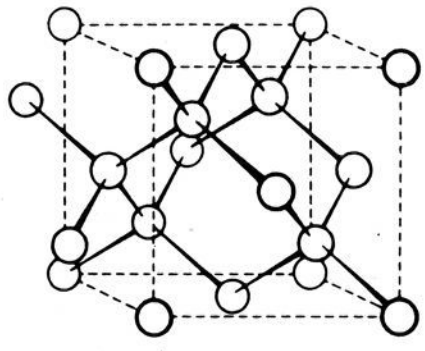

2

was the first organic structure to be completely determined by X-ray diffraction. The molecules are clearly fragments of the solids with the "ends" tied off with the relevant number of hydrogen atoms. Larger fragments of the solid are found in diamantane ($C_{14}H_{20}$) and *anti*-tetramantane ($C_{22}H_{28}$). The organic chemist is quite happy to describe the C–C bonding in terms of a localized bonding model with hybrid orbitals in all three species. The bond lengths in *anti*-tetramantane show[3] an interesting progression, getting closer to that in diamond as the number of coordinated H atoms decreases. Thus CH–CH_2 = 1.524 Å, C–CH_2 = 1.528 Å, CH–CH = 1.537 Å, and C–CH = 1.542 Å. In diamond it is 1.545 Å.

It was only recently that similar fragments of solids have been found for "ionic" materials, although we could regard the structures of the iso- and heteropolyions of the early transition metals as rock salt fragments. **3** and **4** show two views of the structure[4] of the

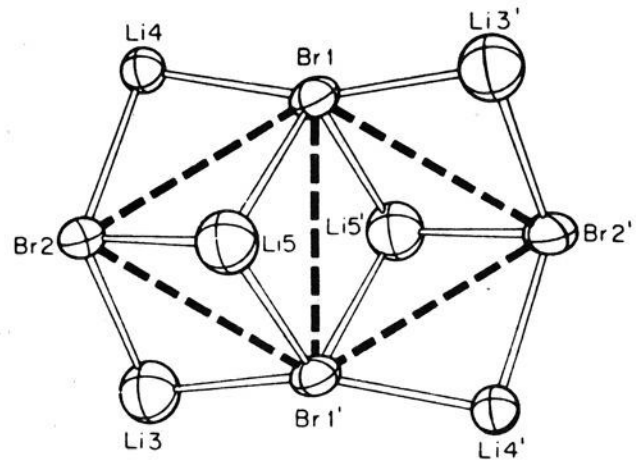

3

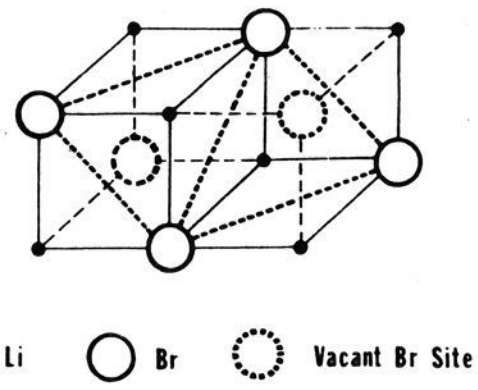

4

cation ($Li_6Br_4(Et_2O)_{10}^{2+}$) formed when phenyllithium reacts with silver bromide in ether solution. (The anion has an interesting structure too but is not relevant to our discussion.) Notice in the second diagram the relationship of the structure to that of a fragment of crystalline LiBr which possesses the rock salt structure. The "ends" of the fragment have been tied off with ether molecules, not shown in our pictures for clarity. These molecules appear to play the same role as the hydrogen atoms in **1**. The average Li–Br distance in this ion is 2.58 (2) Å to be compared with 2.75 Å in the crystal itself. It is interesting to speculate that the cation of **3** and **4** represents the early stage of nucleation of the LiBr crystal from solution. Fragments of metal structures have been known for many years. **5** shows part of a "close-packed" plane of metals with the ends tied off with carbonyl groups in the species $Fe_3Pt_3(CO)_{15}^{2-}$.

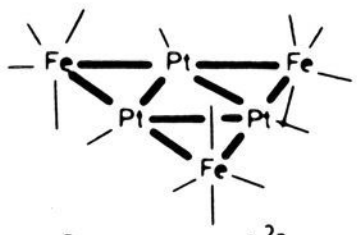

$[Fe_3Pt_3(CO)_{15}]^{2-}$

5

Electron counting is a favorite pastime for inorganic chemists and the recent development of the isolobal analogy has provided an extraordinarily successful tool with which to corral a lot of structural results. But even simpler, the identification of similar arrangements for species with the same electron count (but perhaps rather unconventional chemistry) is also useful. For example, although the coordination of N_2 or azide to a metal center is quite common, there has only recently been a crystallographic characterization[5] of a coordinated N_4 unit in the molecule shown in **6**, $(WCl_5)_2N_4^{2-}$.

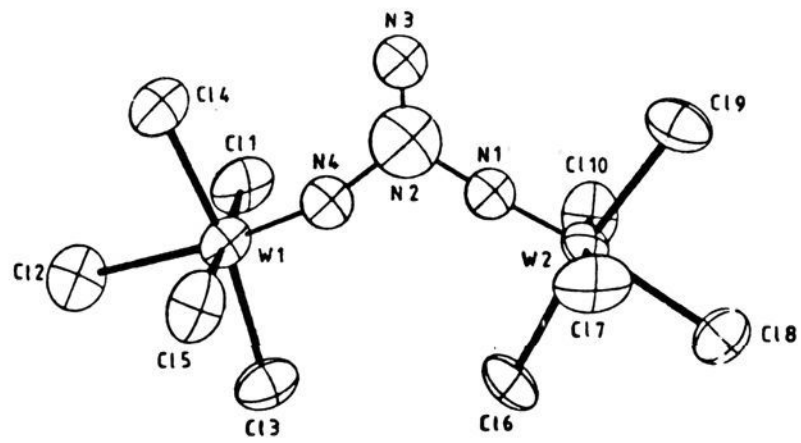

6

This is quite unusual. The bridging N–N distances are 1.23 Å and the terminal N–N distance is 1.49 Å. Rearrangement of the electrons suggests that the species can also be written as $(WCl_5^+)_2N_4^{4-}$. Now N_4^{4-} is isoelectronic with carbonate ion, CO_3^{2-}. Indeed similar local geometries to that found in **6** are found for metal carbonates. Examples include $AgKCO_3$ and the mineral dawsonite, $NaAl(OH)_2CO_3$.

B. Natural Products Inorganic Chemistry

The inorganic world of minerals presents many challenges to the crystallographer.[6] Not least is the finding of a good single crystal for an X-ray study. Although many of these materials are structurally simple, the majority are usually quite complex and present a problem that molecular chemists rarely face. How do you describe them in geometrical terms? How do you relate the collection of (x, y, z) coordinates to an overall picture? In a recent book[7] over 40 pages were devoted to the question of nomenclature in the feldspars alone. The major problems associated with this area are the invariably large number of atoms in the asymmetric unit and that fact that the chemical composition is not simple. Mineral compositions are usually solid solutions of at least two end-members. The combination of these two problems leads to situations that are tough to unravel. Often one particular site may be partially occupied by a variety of different species (usually cations). Thus for example capelenite is

$$(K_{0.05}Ba_{0.04}La_{0.22}Na_{0.10})(Th_{0.04}Ca_{0.15}Y_{5.74}Ce_{0.09})Si_{2.91}B_{6.07}O_{24}F_2$$

with the ions partitioned into the respective structural sites as indicated. This, of course, is an approximation, for cumulative errors in wet chemical analysis and choice of site populations by the crystallographer come into play. An interesting example of such site occupancy is shown in **7**, a potassium lead silicate[8] of for-

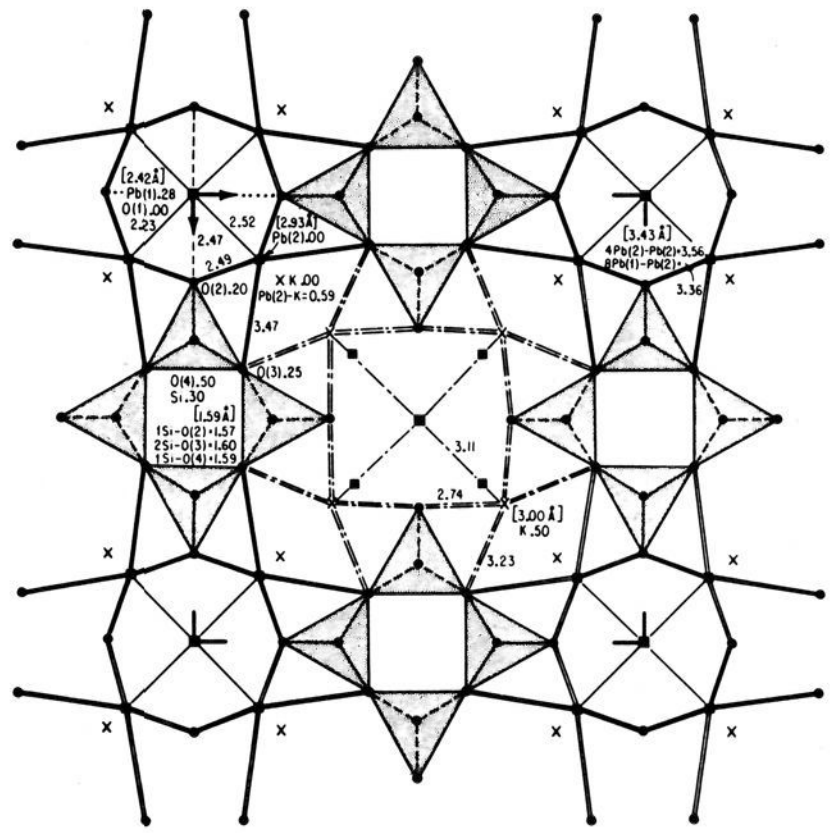

7

mula $(Pb_2O)(Pb_2K_2)Si_8O_{20}$. The material is somewhat peculiar in that on grinding it fluffs up into a mat of very thin fibers. Structurally the lead and potassium atoms occupy the same site in the lattice, as indicated by the second set of parentheses in the structural formula we have written, but there is an interesting twist. The lead atom with its lone pair of electrons leads to a distorted coordination arrangement but the potassium atom defines an undistorted site. The separation of the lead and potassium positions is 0.59 Å.

How the atoms of a given system are ordered over the possible sites of a given structure is an important consideration in this area. For example how the silicon and aluminum atoms order in the feldspars has been an area of active investigation for several years. The problem is a very interesting one crystallographically, since the ordering pattern of the ions is often incommensurate with the translational periodicity of the oxide lattice.[9] In zeolite A however, with a Si/Al ratio of unity it is now established that no two Si atoms and no two Al atoms reside on adjacent sites (Loewenstein's rule) although there have been some claims to the contrary.[10]

Framework silicates containing tetrahedrally coordinated silicon and aluminum constitute a major class of minerals, the feldspars. A closely related type of structure, the zeolites, have found increasing application in the area of catalysis. Particularly important is the presence of channels and large cavities in which chemical reactions may occur, 8. There has been considerable activity in this area in recent years not only in synthesizing new zeolitic materials but in their detailed characterization. Of particular interest has been the determination of the location of water molecules in the structure. (We mention below the determination of a structure containing trapped benzene.) Synthetic hydrated zeolites have not yet been made as large enough

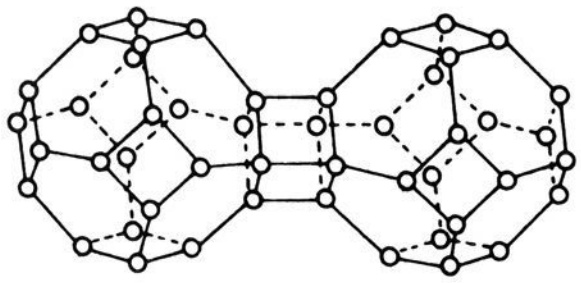

8

single crystals for neutron diffraction to be feasible, and so the few studies that have been undertaken have used naturally occurring material. **9** shows[11] the structure

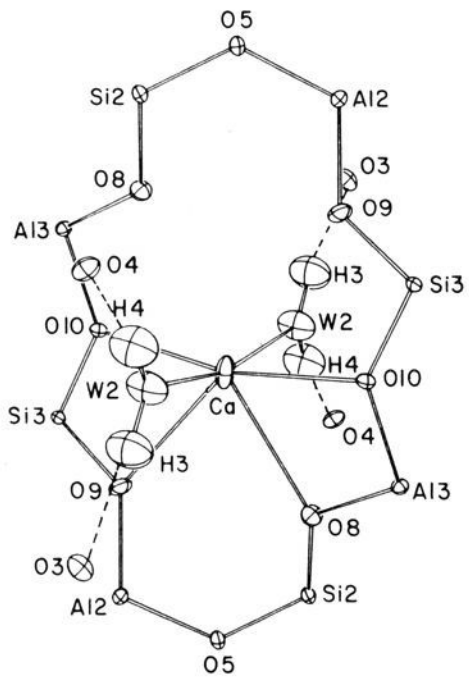

9

of the water molecules which coordinate the calcium atoms in thomsonite, a zeolite with a typical stoichiometry $NaCa_2Si_5Al_5O_{20}\cdot 6H_2O$. In this picture the water oxygens are labeled W and the lattice oxygens O. In many of these systems the ordering of the water molecules is often very complex.

Of considerable industrial importance has been the use of such materials as catalysts of various types for selectively controlling the pathways of chemical reactions, usually at elevated temperatures. One aspect of this field has been the development of shape-selective catalysis, determined by the shape and physical dimensions of the channels and cages in the structure.[12] **10** shows the species cacoxenite,[13] which is not a zeolite but a complex iron phosphate which holds the record for cavity size (14.7 Å free diameter.) It has the rather complex formula $AlFe_{24}O_6(OH)_{12}(PO_4)_{17}(H_2O)_{24}\cdot\sim 21H_2O$, where the last collection of water molecules occupy the large cavity. Cacoxenite is a low temperature phase and on heating rapidly degrades. It is not therefore a viable candidate as an industrial catalyst of the sort just described but could be a suitable host for lower temperature biological reactions such as the replication of DNA.

A few years ago a whole series of crystallographic studies were published which purported to show either zero or under-coordinated alkali or alkaline-earth cations in these zeolite structures.[14] The result attracted considerable attention. For example, the stereoplot shown in Figure 1 appeared in an undergraduate inorganic text[15] along with a discussion of "zero-coordination". The picture apparently shows a rubidium atom floating in space some 4.35 Å away from the nearest oxygen atom. This is 1.56 Å longer than the

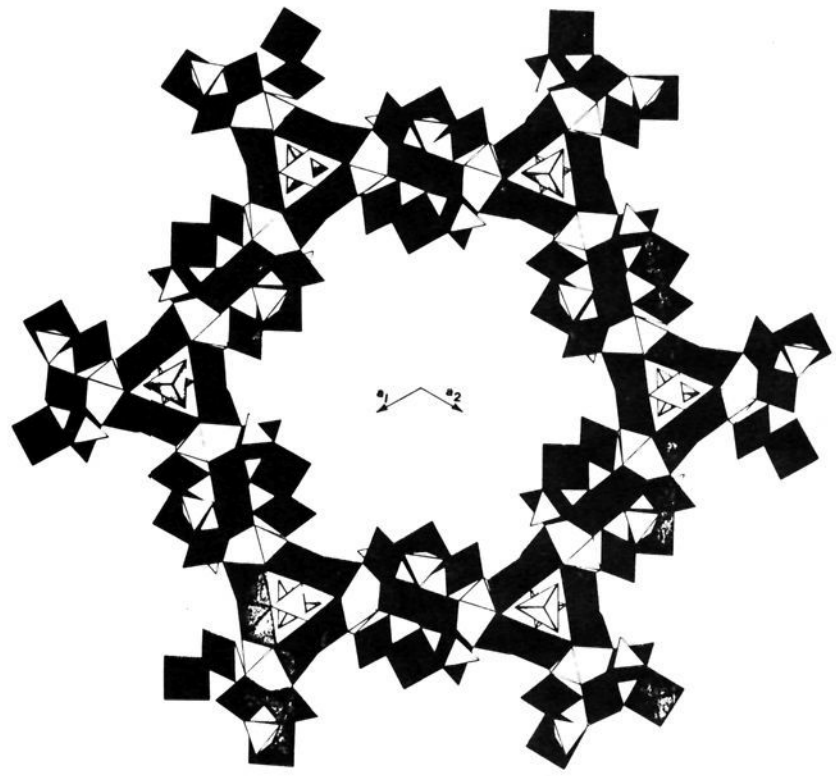

10

sum of the ionic radii for rubidium and oxygen. In fact these results are artifacts associated with the following problems. (a) No independent determination of the chemical composition of the crystal as performed on the crystal used in the X-ray analysis. (b) The supposed zero-coordinate ions are represented by irregular or weak peaks similar in size to residual peaks not ascribed to atoms. (c) A refinement was made for the pseudostructure ($Pm3m$) rather than a superstrucutre with ordered Si and Al ions (see below). Once these questions are taken care of, this density and therefore the ion disappear.[16] The cations do not float like Mohammed's coffin in the structure. In one instance however, a tetrahedrally coordinated AlO_4 ion was found[17] in the center of the sodalite unit.

Some recent studies have actually identified the geometrical arrangement of neutral molecules trapped in zeolites. **11** shows how the benzene molecule lies in the zeolite, sodium Y, as determined by powder neutral diffraction.[18] Although these experiments pushed this technique close to its limits, the general picture is a clear one. As the temperature of the sample is lowered, the benzene molecules order in the silicate cages.

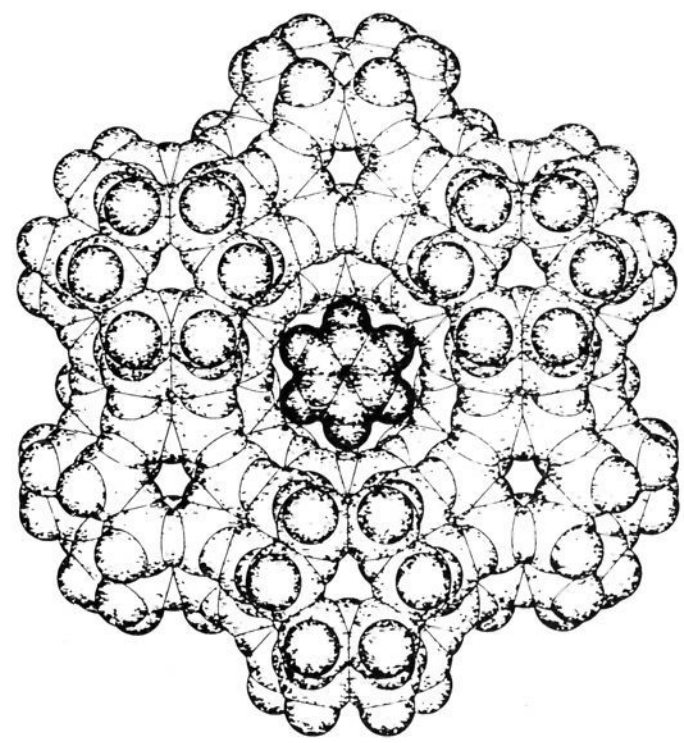

11

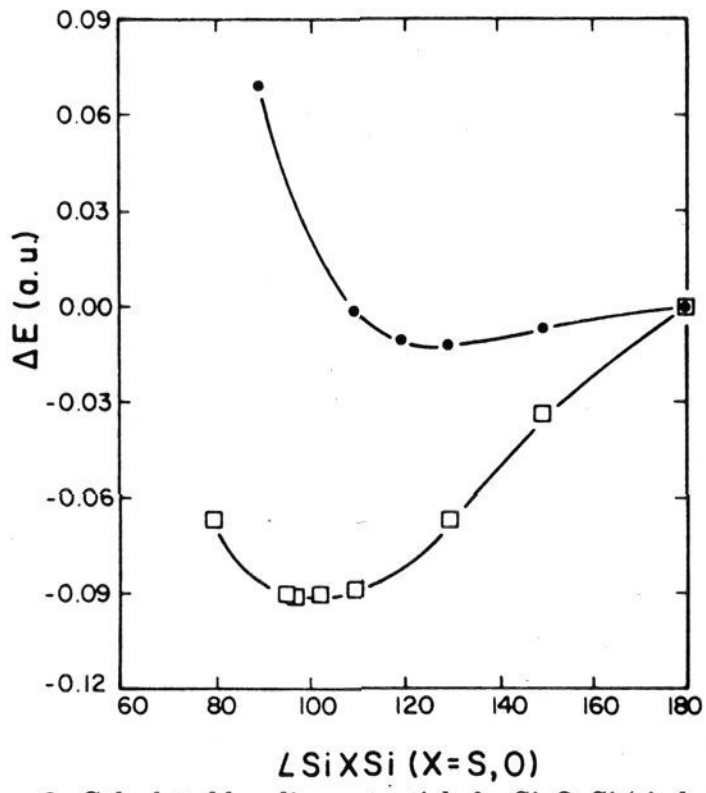

Figure 2. Calculated bending potentials for Si–O–Si (circles) and Si–S–Si (squares) units. (Reprinted with permission from ref 20. Copyright 1981 Springer-Verlag.)

Not only is knowledge of the geometry of coordinated water important, but so is that of the metal ions in the structure. Both certainly play a very important role in determining the structure of the zeolite itself. **13** shows

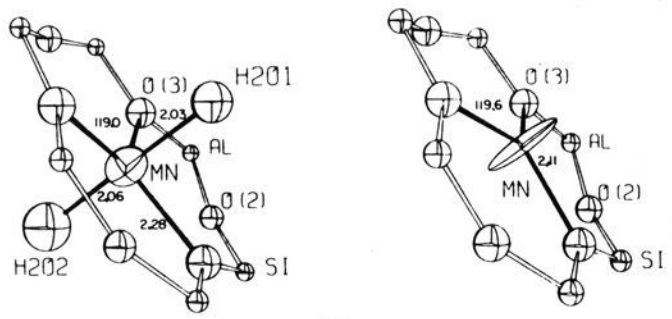

12

the coordination[19] of manganese in hydrated and dehydrated zeolite A. (The large asymmetry of the thermal motion may represent a problem with the refinement of the latter.) A technique which may prove useful in determining the positions of these ions accurately is that of anomalous dispersion which would employ the resources of a synchrotron.

One very striking feature of the crystal chemistry of the natural world is the great variety of structures described as silcates of some type. A comparable chemistry for the sulfur analogues for example does not exist. We can associate a part of this diversity with a rather interesting structural feature, and that is the soft bending potential at the oxygen atom. Since it costs little energy to distort the geometry at this center, the number of otherwise uncomfortable structures (in terms of strain energy) which exist is quite large. Figure 2 shows calculated bending potentials for Si–O–Si (circles) and Si–S–Si (squares) units.[20] Notice the softer potential for oxygen and also a minimum at a larger Si–X–Si angle for oxygen compared to sulfur. It is fascinating to realize that the origin of the vastness of natural product inorganic chemistry lies in such a simple feature. Figure 3 shows how a histogram describing the frequency of the experimental occurrence of Si–O–Si angles from a large database of materials correlates very nicely with the curve expected using a Boltzmann distribution with the calculated potential.[21]

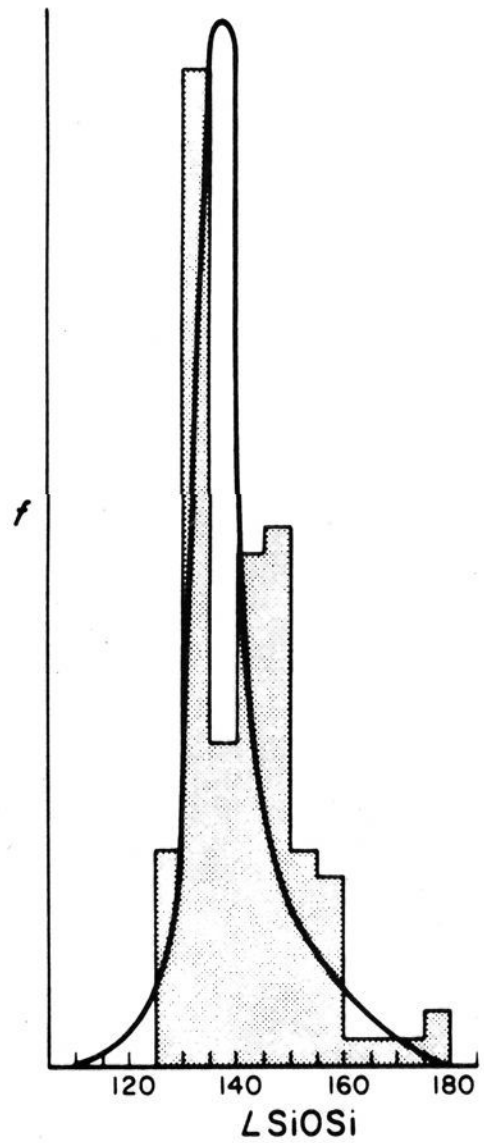

Figure 3. A comparison of the Boltzmann weighted SiOSi angle distribution function calculated for $H_6Si_2O_7$ with an experimental frequency distribution. (Reprinted with permission from ref 2. Copyright 1981 Academic Press.)

Two models have been used to understand these observations. The first turns on its head the traditional concept concerning the sizes of anions and cations when next-nearest neighbor interactions are involved. Whereas the conventional view (which we discuss in Section IIC) of the relative sizes of ions has been governed by prescriptions for building structures which insert small cations into a lattice of large anions, it has been ably argued[22] that as far as the nonbonded radii of atoms are concerned, it is the cations which are considerably larger than the anions. Two views of the structure of the Si_8O_{20} unit which emphasize this point are shown[23] (**13**). One shows regular, vertex-connected

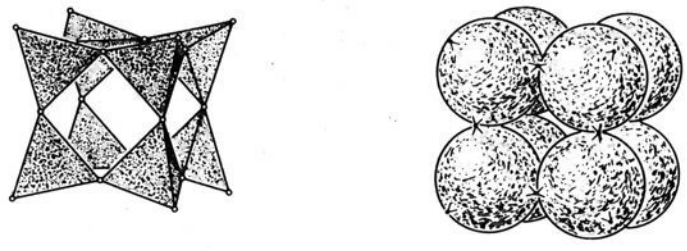

13

SiO_4 tetrahedra. The other shows in addition spheres at the silicon positions drawn with the nonbonded radius. For the case of silicate chemistry it has been pointed out that the Si–Si nonbonded distance is relatively constant (3.06 Å) across a whole spectrum of structures. Such an observation could be interpreted in the following way. The closest distance between two silicon atoms before they significantly start to repel each other via the switching on of overlap forces is close to 3.06 Å. In other words, it is these nonbonded repulsions which control the structure. Evidence for a soft bending

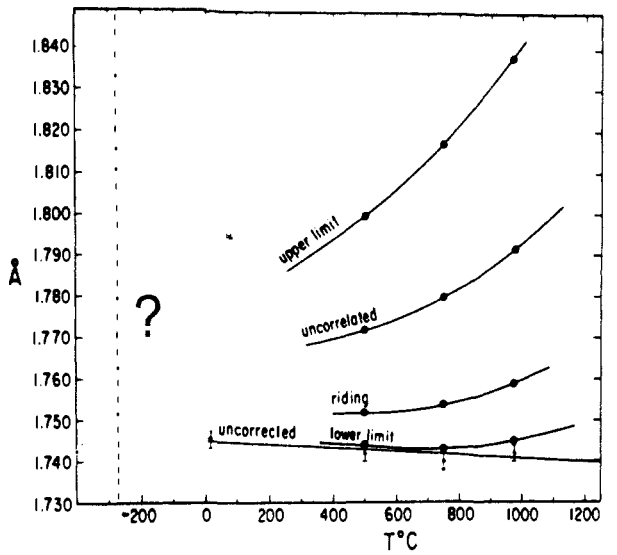

Figure 4. The model dependence of Al-O distance in albite. (Adapted from ref 30).

motion also comes from a study of the radial distribution function for glassy SiO_2. The peaks due to Si–O and O–O distances are quite sharp but that for Si–Si is broad.[24]

The other approach employs exactly the same arguments we will develop in section IV for understanding the structures of oxides containing planar three- and four-coordinate anions. Strong π bonding between the oxygen and silicon atoms favors[25] a linear geometry for the Si–O–Si unit. σ bonding favors a bent unit and a compromise arrangement with a soft bending potential is the result. In the three- and four-coordinate case a soft bending potential at oxygen is not apparent, although in the anatase structure there is considerable thermal motion perpendicular to the OTi_3 plane determined[26] via room temperature diffraction studies. A group of molecules with analogous properties to the ···Si–O–Si··· unit is carbon suboxide and their phosphine substituted analogues. Here there is a very low frequency bending vibration[27] associated with the (OC)–C–(CO) or (R_3P)–C–(CO) arrangement, which may also be interpreted in terms of π bonding to the central atom by the ligands.

Chemists are prone to comparing their experimentally determined crystal structure with parameters calculated via some quantum mechanical method. However, the experimental results are for a warm (hot compared to absolute zero) sample where the atoms are in motion whereas the theoretical results are for a molecule with no zero point energy at all. The inclusion of vibrational motion into the crystallographic problem for an anharmonic oscillator, and especially one with a soft force constant, is hardly a routine matter. In silicate chemistry where bending around the oxygen atom fits this description, we might well expect to see some significant changes in the determined structural parameters with temperature. Of course as the system is cooled the crystal will contract but how will this manifest itself in changes in the interatomic distances? Figure 4 shows some data for albite[28] to illustrate the importance of the effect. The interpretation of the behavior of the Al–O bond length at higher temperatures is critically dependent on the nature of the unknown vibrational correlations. Obviously the distance to use when

TABLE I. Bond Lengths in Cristobalite

	10 K	473 K
Si–O(i)	1.602 (1) Å	1.605 (2) Å
Si–O(ii)	1.617 (1) Å	1.590 (2) Å
Si–O–Si	144.7 (1)°	148.4 (1)°

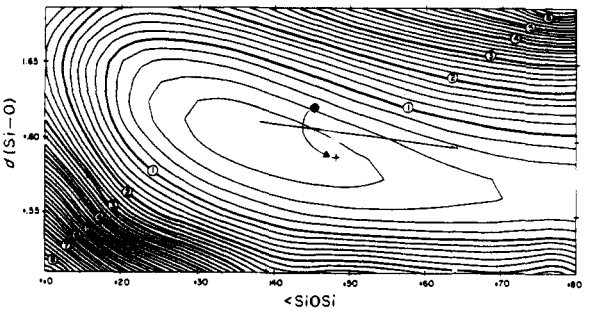

Figure 5. Ab initio calculations on silicate fragments. (Adapted from ref 2.)

making comparisons with theory is that extrapolated to 0 K. Table I shows some recent results[29] for cristobalite. It shows quite a difference in interatomic distance with temperature. The effect of temperature and pressure on crystal structure have been considered in some detail for several classes of systems.[30,31] Figure 5 shows the results of some ab initio calculations on silicate fragments.[32] The solid line shows the bond length/bond angle correlation obtained from a large number of room temperature crystal structure determinations on a variety of silicates and the contours of the computed energetics of the distortion. Notice that the solid line does not sit exactly in the computed valley. Also shown is the temperature behavior of one of the Si–O distances of Table I. The solid cross shows how the point indicated by the circle moves on cooling. It clearly is more in accord with the theory. We should be cautious of course in making any broad claims with just a single point, but the observation is an interesting one and suggests that there is a case to be made for all comparisons with theory to be made with low temperature data.

The natural and synthetic worlds are full of materials that have somewhat unusual structures. Often when they are uncovered they are the forerunner of other similar species which are discovered or synthesized later. The molecule ferrocene, for example, falls into this category. Other species are sometimes so unusual that we often wonder whether the crystallographic determination is correct. In this case only time will tell. Silica-w is a system that falls into this class. The identification of this material relies on a powder pattern study.[33] This species is interesting since it contains chains of edge-sharing tetrahedra, **14a** with particularly close O–O and Si–Si distances. A disturbing feature of the structure however is the presence of very long Si–O distances. These are longer than the distances expected for six-coordinate silicon. In stishovite (SiO_2 in the rutile structure) the average Si–O distance is 1.78 Å. Edge-sharing chains of this type are quite well known in sulfur chemistry. SiS_2 has this structure and there are many "infinitely adaptable" structures that contain FeS_2 and other metal units in a similar arrangement. The results of numerical calculations have been used[35] to shed doubt on the existence of this species, but the molecule **14b** has recently been synthesized.[36] A P_2O_2

analogue is also known.[37] A modern structural reinvestigation of silica-w is clearly in order.

14a

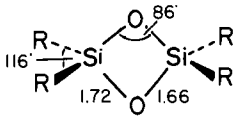

R = Mesityl

14b

Silicon in an environment where it is six-coordinated by oxide is also very unusual. Six-coordination by oxide is found in stishovite, a high-pressure polymorph of SiO_2, in a few complexes, and in two polymorphs of $Si_2P_2O_7$. Even rarer is coordination by hydroxide. The complex low-temperature mineral thaumasite (from the Greek meaning marvel), $[Ca_6[Si(OH)_6]_2 \cdot 24H_2O](CO_3)_2(SO_4)_2$, exhibits[38] the only known example. The Si–O distance is 1.78 (3) Å.

C. Description of Crystal Structures

We have already mentioned the problems associated with the geometrical description of crystal structures. This is in fact a very large stumbling block for understanding solids. If we cannot describe, organize, and categorize structures geometrically, we are at an immediate disadvantage in appreciating their electronic stability. Recall the tremendous progress made in synthetic organic, especially natural product, chemistry as a result of the appreciation of geometric relationships. Molecular chemists usually write the structures of molecules using traditional ball-and-spoke models such as those of 1 and 2. This is simply because our chemical prejudices associate close internuclear contacts with chemical bonds.

The traditional way of looking at the structures of solids containing extended arrays is to build them up from cation centered polyhedra which may be linked to each other by vertices, edges or faces, or various combinations of these modes. Dumortierite has a structure that contains[39] examples of all three modes. This also provides a useful way of visualizing structures too, although the emphasis on the cation rather than anion coordination geometry is often misleading. Another pictorial aid is to describe structures in terms of the cation occupancy of the interstices generated by a pseudo close-packed array.[40] The anion arrangement of many structures approximates one of the sphere packings, of which the face-centered cubic, and hexagonal close-packed are the best known. Since such a concept assumes spheres of fixed size in contact, it forces a chemical interpretation onto a purely geometrical approach. A better term is perhaps eutaxy (from the Greek meaning well-ordered) which defines an arrangement[41] of atoms whose centers are at the centers of the spheres of a close-packing. We will be even more general in this article and refer to the more and less electronegative atoms in the crystal as anions and cations, respectively, without any implication of "ionic" bonding in the material.

Structures 15–17 show three different ways to occupy

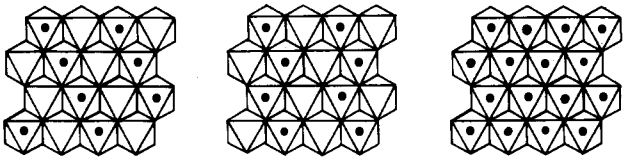

15 16 17

the octahedral interstices of a hexagonal close packed array for an oxide of stoichiometry MO_2. Overall, half of the holes need to be occupied. In 15 and 16 the set of interstices between every adjacent pair of sheets is half-occupied (... $^1/_2$, $^1/_2$, ...) but in 17 every other set if completely empty (... 0, 1, ...). The three-dimensional structures that result are respectively the rutile (TiO_2), α-PbO_2, and CdI_2 structures. These drawings show the connectivity of the structures but give us no information about the real geometries of these systems. For example the rutile structure, if it were based on an undistorted hexagonal eutactic array, would be orthorhombic with a pyramidal geometry at oxygen. (This is the $CaCl_2$ structure.) In fact the anion array has relaxed such that the geometry at oxygen is rigorously planar and the crystal is tetragonal. The geometry at the metal site is interesting too. In TiO_2 there are two long and four short Ti–O distances,[26] but in CrO_2 with the same structure type the converse is true. Use of the approach in structures 15–17 is very useful in the field of combinatorics[42] to systematically generate all the possible ways of filling the interstices of such arrays and hence enumerate possible structure types.

Polyhedral diagrams (18–20) are shown of the three structures. Notice immediately that whereas 18 and

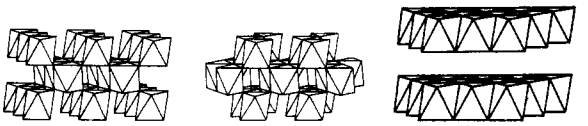

18 19 20

19 are framework structures, 20 is a layer structure. Since we can readily imagine that the interlayer forces are weaker than the intralayer ones, polytypes which only differ in the orientation of one slab with respect to the next should be possible. Indeed cadmium iodide is known to crystallize in a large number of such polytypes.[43] If the anions are in cubic eutaxy, the structure is often termed the cadmium chloride arrangement. Thus this layer structure in general can be called the cadmium halide type. In all three structures the octahedra share edges with each other. Structures 21 and 22 are ball-and-stick pictures for 15 and 17. They are more cluttered than the other drawings but do show the planar anion geometry found in the rutile structure and the pyramidal one in the CdI_2 arrangement. All three of these approaches have their uses in organizing and understanding the structures of crystals. There are of course other ways of viewing the structures of solids. One of the most recent developments has been the use of the concept of minimal surfaces[44] in an effort to relate crystal structure with modern topological ideas. We shall comment again at several places in this article on these three, deceptively simple, structures, 15–17.

As we have mentioned, the structures of many materials have been described in terms of the linking to-

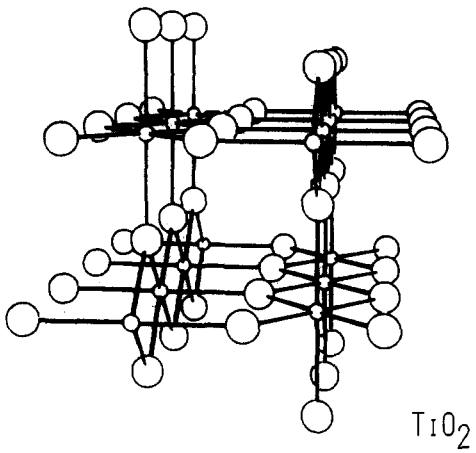

21

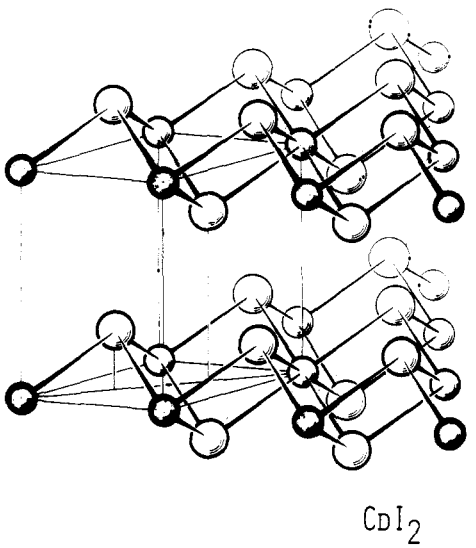

22

gether of cation-centered polyhedra. In many cases this has led to a geometrically satisfying description of the structure. In many others however, such an analysis has proved little help. As Wyckoff has written "Although many complicated salts ... have fundamentally simple structures, there are numerous others which bear no obvious relation to the simpler arrangements."[45] Striking examples of such materials include sulfates of the uni- and divalent metals. $BaSO_4$ (barite) is an example of this type. The oxide ion arrangement is far from being a close-packed one and the structure is dominated by the apparently arbitrary way the sulfate tetrahedra are packed in the crystal. In many cases (K_2SO_4 is a notorious example) there are several polymorphs in close energetic proximity with rather subtle and difficult to understand geometrical relationships. Problems such as this have led O'Keeffe and Hyde to point out[46] another relationship which is an extremely useful one in geometrically describing and classifying structure type. In their approach the oxide ions are ignored and the structure of the resulting cation array studied. Fascinatingly, the result very often corresponds to that of a well-known alloy system. In other words, instead of traditionally regarding a structure as a regular anionic lattice into which cations have been inserted, the alternative is used, namely that of inserting anions into a regular cation array. Structures **23** and **24** show how the approach works for the barite struc-

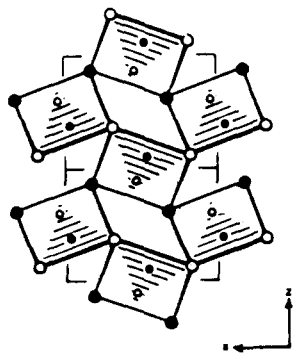

23

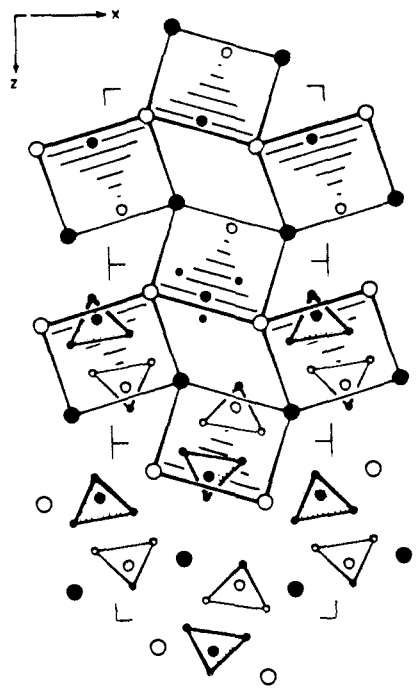

24

ture. The array of Ba + S atoms is simply that of the well-known FeB alloy structure (**23**) with Ba (larger circles) in place of Fe and S in place of B. The oxygen atoms then are inserted into SBa_3 tetrahedra. Structure **24** shows this descriptive viewpoint at the top and the older one at the bottom. (Large, medium, and small circles represent Ba, S, and O, respectively.) Contrast this with a way of describing the structure of $NiWO_4$ for example. Here the Ni and W atoms are inserted into half the octahedral interstices of a close-packed array of oxygen ions.

We may use such ideas to shed fresh light on phase transformations in solids which would be difficult to understand in other ways. One particularly interesting one[46] is the olivine to spinel transformation under pressure for a material such as the olivine forsterite (α-Mg_2SiO_4). The Mg_2Si array in olivine is simply that of the Ni_2In structure, where the oxygen atoms are inserted into holes to produce SiO_4 groups. Structure **25** at left shows the $SiMg_6$ trigonal prisms of such a structure and at the right the traditional description in terms of SiO_4 tetrahedra. (Large, medium, and small circles are Mg, Si, and O, respectively.) The corresponding $SiMg_2$ array in the spinel structure is the

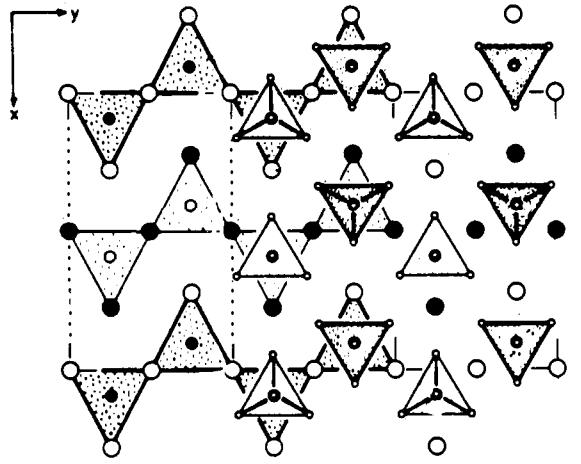

25

$MgCu_2$ cubic Laves phase, the copper atoms of which are shown at the left of structure **26**. The SiO_2 tet-

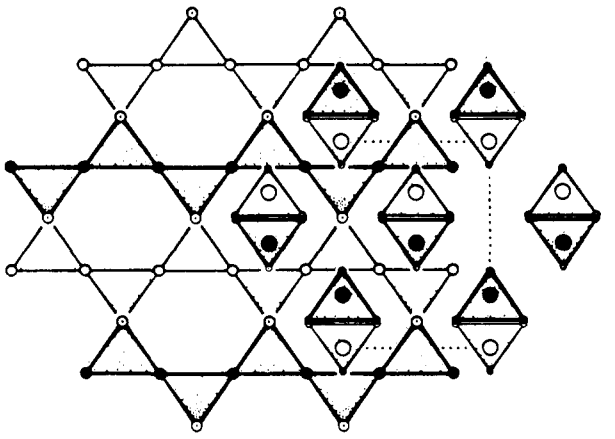

26

rahedra are similarly located with respect to the atoms of these chains in both structures. It is the metal atoms which are displaced when going from one to the other. Notice that the coordination numbers of the cations *by cations* have increased during the transformation. Accordingly the Mg···Mg and Si···Si distances have increased but the Mg···Si distance has decreased. Such behavior is typical of phase transformations where there is a change of coordination number. For example in NaCl, proceeding from the six-coordinate rock salt to the eight-coordinate CsCl structure, the Na—Cl distance increases, but the Cl···Cl and Na···Na distances decrease. In the olivine to spinel transformation the Mg—O and Si—O distances hardly change, nor does the primary coordination of cations *by anions* change. This has made this phase transformation difficult to understand. The oxygen atoms in fact appear somewhat irrelevant in a geometrical sense to the transformation. Such insight would not have been obtained if the usual model, namely insertion of cations into anionic arrays, had been used.

If the emphasis on the cation ordering can help us categorize a stoichiometrically simple structure such as that of barite, can it be used to look at some of the horrendously complicated materials often found in complex oxide chemistry? Scheme I shows a structural tree[47] which is rather beautiful in its simplicity and descriptive content. The atomic coordinates in one of the polytypes (Θ) of Ni_2Si are similar to those of α-iron,

SCHEME I

α-Fe bcc structure $Im3m$

↓

α-Fe rhombohedral cell, $R\bar{3}2/c$
(FeFe) $(FeFe)_2$

↓

Θ-Ni_2Si
(NiNi) $(NiSi)_2$

↓

glaserite $NaK_3(SO_4)_2$
(KNa) $(KS)_2$ O_8

↓

fillowite $Na_2CaMn_7^{2+}(PO_4)_6$
({X}{X}) $(\{X\}P)_2$ O_8

where $\sum\{X\} = Na_{2/3}Ca_{1/3}Mn_{7/3}^{2+}\square_{2/3}$

especially if the latter is referred to a rhombohedral cell as in the first step. Ni_2Si is then a "coloring" in two different colors of the bcc lattice. (In an analogous way the sphalerite, or zincblende, structure is a coloring of the cubic diamond structure.) Glaserite, quite a complex species,[48] is difficult to describe by using the conventional approach but is very conveniently described in terms of a "stuffed" Ni_2Si arrangement, the oxygen atoms lying in interstices in the structure. The fillowite ($Na_2CaMn_7(PO_4)_6$) arrangement[49] is even more complex. Now the sites of the alloy structure are occupied incompletely by a collection of different ions. The presence of an ordered vacancy is written as □. Although Scheme I does not show it, the collection of metal ions {X} in fillowite are actually ordered over the array defined by the atomic positions of α-Fe. An analogous structure in terms of anionic arrays is that of NbO. This could be written $Nb_{3/4}O_{3/4}\square_{1/4}$ to emphasize the vacancies in the close-packed oxide array. Nb atoms then fill three-fourths of the octahedral holes (coordinated by four oxygen atoms and two vacancies) so generated. We spare the reader the details of the geometries of these species but show only a part of the published structure[49] of fillowite, **27**, which gives a good feel for the complexity of the arrangement. Structural relationships such as those in Scheme I require considerable skill to generate and rely initially on the comparison of the axial ratios of complex solids with those of perhaps unconventional projections of simpler materials as suggested by group/subgroup relationships.

III. Simple Structural Models

A. Bond Valence Sum Rules

The prediction of crystal structure is difficult, although as we will show in section IV the variation in structure with electron count for a particular series of systems may often be understood. A related problem is the prediction of interatomic distances, and certainly the factors which determine a particular crystal structure are a combination of "electronic" factors and the relative "sizes" of the atoms as measured by their bond lengths to other atoms. There is one particularly useful way in which the bond lengths of a subset of crystal structures may be approached, which is a development of Pauling's second rule. In solids which are not of the metallic, organometallic, or van der Waals types (i.e.

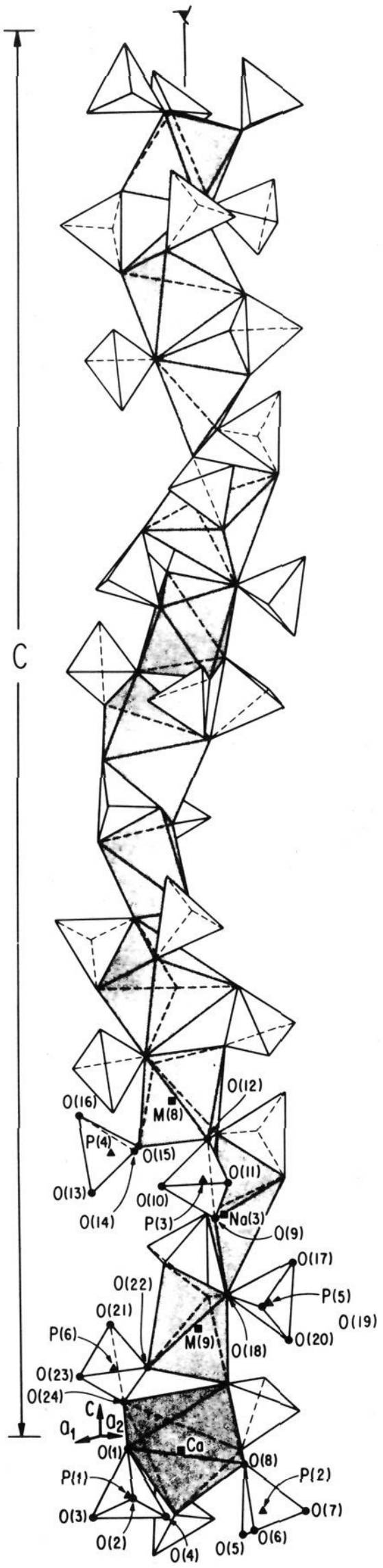

27

those where either the delocalized model has to be used or the interactions are weak) a useful concept[50–53] is the bond valence s, which is determined by the interatomic separation or bond length r. Two expressions are commonly used to link the two

$$s = (r/r_0)^{-N} \tag{1}$$

and

$$s = \exp[(r_0 - r)/B] \tag{2}$$

where r_0 and N or r_0 and B are constants for a particular atom pair. A remarkable feature of the bond valences of known crystal structures is that their sum around a particular anion or cation (i) to its coordination cations or anions, respectively (j) is a constant. This is set, by definition, equal to the traditional valency (V_i) of the species viz.

$$V_i = \sum_j s_{ij} \tag{3}$$

Equation 2 is somewhat more useful in that B is remarkably constant (0.37) for a wide range of systems. This leaves a single variable (r_0), which may be expressed[53] in terms of additive parameters for anion and cation. Equation 3 therefore controls the way the remaining interatomic distances around a given atomic center change when one particular distance is increased or decreased. It also gives a feel for the relative strengths of contacts of various types. Six-coordinate sodium will form bonds with a bond valence of approximately one-sixth, and four-coordinate nitrogen (envisaged as N^{3+}), bonds with a bond valence of approximately three-fourths. These numbers (the "valency" divided by the coordination number) are termed the electrostatic bond strengths to avoid confusion with the definitions above.

Consideration of these equations has been extremely important in crystal chemistry. In crystal structure determination it has been a very useful indicator of those oxygen atoms with coordinated hydrogen atoms which have been missed by the X-ray diffraction experiment. Such oxygen atoms will have low bond valence sums when only the contacts to the detected atoms are used. It is still probably the primary means to distinguish oxide and hydroxide species in crystals. The rule has impact, too, on the determination of site preferences in mixed systems. For example consider the ordering of the lithium and magnesium ions over a close packed array of oxide (–2) and nitride (–3) ions in LiSiON. In one particular coloring of the lattice[54] there are two types of tetrahedral cationic site generated. We may then ask which ion resides in which site out of **28** and **24**? Evaluation of the electrostatic bond

28 **29**

strength sums to each site indicates that the oxide will enter the site in **28** since the sum here to X (ebs = 1.75) is closest to 2. The distances to oxide may be somewhat shorter perhaps since the ion is undersaturated in Pauling's language. Similarly the nitride ion should enter the site Y in **29** with the bond strength sum (ebs = 3.25) closest to 3 and with somewhat longer distances (i.e. oversaturated).

The use of eqn 3 alone is insufficient to fix the topology of the crystal structure, but Brown has found[52] that there is another rule which works well. This may be stated in two equivalent ways. (i) The individual bond valences around each center will tend to be as

TABLE II. Prediction of Bond Lengths in Diopside, $CaMgSi_2O_6$

	network			
	valence, vu	Brown[52] length, Å	Baur[55] length, Å	observed length, Å
Si–O(1)	1.07	1.60	1.62	1.60
Si–O(2)	1.17	1.56	1.59	1.58
Si–O(3)	0.88	1.67	1.67	1.66
Si–O(3)	0.88	1.67	1.67	1.69
σ(Si–O)		0.01	0.01	
Ca–O(1)(×2)	0.32	2.35	2.43	2.36
Ca–O(2)(×2)	0.42	2.24	2.32	2.35
Ca–O(3)(×2)	0.12	2.80	2.62	2.56
Ca–O(3)(×2)	0.12	2.80	2.62	2.72
σ(Ca–O)		0.14	0.07	
Mg–O(1)(×2)	0.30	2.15	2.10	2.12
Mg–O(1)(×2)	0.30	2.15	2.10	2.06
Mg–O(2)(×2)	0.40	2.01	2.06	2.05
σ(Mg–O)		0.06	0.02	

nearly equal as possible. (ii) The sum of the bond valences around any closed loop in the structure will be equal to zero (if we define a bond valence from anion to cation as being positive, and one from cation to anion as being negative.) There are obvious links between this second formulation of the rule and Kirchoff's rules for electrical circuits. Baur has developed[55] a similar method for ensuring that the valence sum rule is obeyed. These ideas have led to a search for a method[56] for the systematic generation of possible crystal structures which fit these rules. Such a general algorithm does not yet exist, but its development would be an extremely useful one for inorganic chemists. As an example of how good the bond-valence method is in predicting both large and small distortions, we show in Table II observed and predicted distances[52] in diopside, $CaMgSi_2O_6$, using both Brown's and Baur's methods.

Let us ask how the bond-valence rule could work with simple orbital ideas.[57] We may use the angular overlap model[58] to evaluate the molecular orbital stabilization energy of a two center–two electron bond (as in an M–O linkage in a metal oxide) as

$$E_{stab} = -(H_{ij})^2/\Delta E + (H_{ij})^4/(\Delta E)^3 \quad (4)$$

where H_{ij} is the interaction integral between the two orbitals concerned and ΔE is the zeroth-order energy separation, controlled by the electronegativity difference between them. The H_{ij} depend upon the geometric details too. Assuming that H_{ij} varies with distance as r^{-m}, then

$$E_{stab}(r) = -(J^2/\Delta E)(r^{-2m}) + (J^4/(\Delta E)^3)(r^{-4m}) \quad (5)$$

J is a parameter dependent on the identity of the atoms comprising the linkage. The equilibrium distance r_e is simply given by

$$r_e^{2m} = 2(J^2/(\Delta E)^2) \quad (6)$$

If now the O atom is coordinated by α equivalent linkages, we may show that now per linkage

$$E_{stab}(r) = -(J^2/\Delta E)(r^{-2m}) + \alpha(J^4/(\Delta E)^3)(r^{-4m}) \quad (7)$$

with

$$r_e^{2m} = 2\alpha(J^2/(\Delta E)^2) \quad (8)$$

Now of course we may scale the internuclear separation by the introduction of a constant r_0 and write a new dimensionless function

$$(r_e/r_0)^{-2m} = (1/2\alpha)(\Delta E/J)^2 r_0^{2m} \quad (9)$$

the left-hand side of which is very similar to the expression of eqn 1. Summing all such terms for the α-coordinate atom leads to

$$\sum(r_e/r_0)^{-2m} = (1/2)(\Delta E/J)^2 r_0^{2m} = \text{constant} \quad (10)$$

Identification of $2m$ with the N of eq 1 and the constant with the traditional valency V completes the picture. Elsewhere[57] we show how Brown's rule follows from this treatment.

TABLE III. The Valence Sum Rule in $Ca_{5.45}Mo_{18}O_{32}$

repeat unit i	no. of units	valence of Mo V_i	anion charge (q) per repeat
MoO_3	2	3.74 (5)[a]	2.26
$Mo_2O_{3.5}$	4	3.42 (2)	0.22
		3.36 (3)	
Mo_4O_6	2	2.20 (1)	2.65
		2.47 (4)	
total charge			10.7

[a] There are five different units in the crystal (labeled 1–5) with these stoichiometries.

A very nice illustration of the utility and self-consistency of the method is shown in the following example. McCarley and co-workers have synthesized a new ternary oxide of stoichiometry $Ca_{5.45}Mo_{18}O_{32}$ whose structure[59] is rather complex. There are five different molybdenum environments in the crystal shown in Table III. We may use the observed Mo–O distances to evaluate the "valency" of each of these different Mo atoms (V_i) by using eq 3. (An error of 1 standard deviation in the Mo–O distance makes an error of 0.01–0.02 in the bond strength sum.) These are shown in column 4. The anion charge on each repeat unit is simply given by evaluating the expression

$$g = \sum_i n_i V_i - 2m_i \quad (11)$$

where n_i and m_i are the number of metal atoms and oxygen atoms in the ith unit. On summation the total anion charge is found to be 10.7. The cation charge from the stoichiometry is simply $2 \times 5.45 = 10.9$. The close similarity of the two numbers is very striking.

If the valence strength represents in some way the strength of chemical bonding,[60] then its variation as the geometry of the structure is changed should map out the potential well for atomic motion around that ion, namely the anisotropic thermal motion.[61,62] Let us assume that all the strong bonds in a crystal have been included, and now we put into this lattice the ions which are less strongly bonded. We may sample the space in the crystal at each point calculating a new function

$$D = (\sum_j s_{ij}/V_i)^{-q} \quad (12)$$

which, if q is chosen to be about 16, produces a map which looks strikingly like the atomic probability density maps found in the diffraction experiment. D will only be unity at an equilibrium atomic position where $\sum_j s_{ij} = V_i$. Figure 6 shows a comparison[62] for α-AgI at $z = 0$. At the left in Figure 6 is the neutron diffraction difference map and at the right in Figure 6 is that

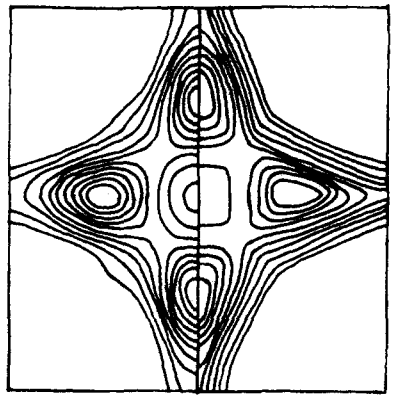

Figure 6. Neutron diffraction difference map (left) and that predicted from the valence map (right). (Reprinted with permission from ref 62. Copyright 1982 Academic Press.)

predicted from the valence map. If the "valence density map" does correlate with the potential energy of the atomic motion, then their examination should indicate those pathways for ion movement. (Recall that α-AgI is an ionic conductor.) The surface for $D = 1$ is that which satisfies eq 3 exactly.

B. The "Ionic" Model and Structures of Solids

We begin with the old viewpoint associated with the names of Bragg, Goldschmidt, and Pauling[63] that so-called "ionic" materials are assembled in the following way. The anions (formed from the more electronegative atoms present) form a close-packed three-dimensional array in which the small cations (the least electronegative atoms) occupy the tetrahedral and octahedral holes of such a framework. According to Pauling's first rule, each ion may be assigned a radius r_i such that the AB distance in a crystal is simply $r_A + r_B$. Which type of interstice is occupied is determined by the radius ratio of anion to cation (ρ). This is Pauling's second rule. The sharing of the edges or faces of the cation-centered polyhedra so generated is energetically unfavorable since it forces the positive charged cations to lie closer to each other than if such polyhedra shared vertices (Pauling's third rule). On Coulombic grounds therefore the ordering of the cations in the interstices of the anion array will be such as to avoid this juxtaposition. (Sometimes, of course, the stoichiometry of the system forces the sharing of polyhedral elements. An example is the rock salt structure where all the edges of both anion and cation centered octahedra are shared.) These statements, formalized by Pauling in his famous rules, introduce the concept of atomic or rather ionic size. Although it is true in general that larger ions (as evidenced by longer bonds to oxygen for example) invariably have a larger coordination number than smaller ions, this is a vague statement compared to Pauling's who assigned critical radius ratio values to define the boundary between different coordination numbers.

Figure 7 shows the gist of his argument. If too many anions are packed around a cation, then anion–anion repulsion becomes large enough to prevent close anion–cation contact. If r is too larger, then a small cation will "rattle" in the interstice. Since anion–cation interaction is stabilizing, such a structure may be less stable than a structure with a lower coordination number. Given a collection of hard spheres of radius r_- in

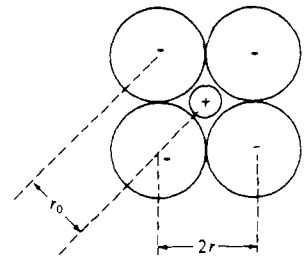

Figure 7. Determination of crystal radii.

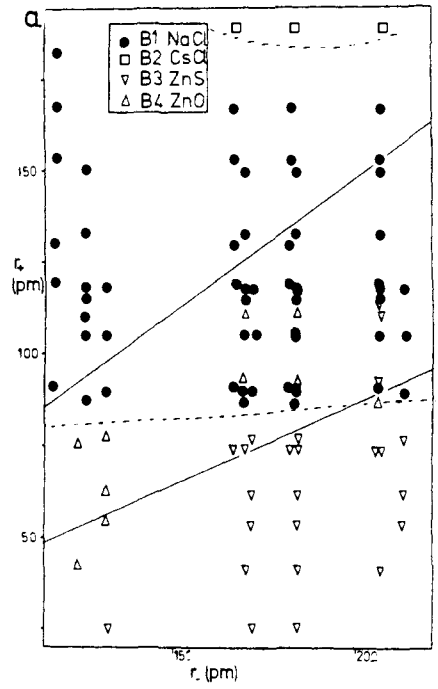

Figure 8. A structural sorting map for AB octets using ionic radii as indices. (From Burdett, J. K.; Price, S. L.; Price, G. D. *Solid State Commun.* 1981, *40*, 923. Copyright 1981 Pergamon Press.)

contact, the radius of a tetrahedral role in the anion lattice is $0.225r_-$, that of an octahedral hole is $0.414r_-$, and that of a cubic (eight-coordinate) hole is $0.732r_-$. So for the anions and cations to be in contact without strong destabilizing repulsions between the anions the radius ratio $\rho = r_+/r_-$ should be in the range $0.414 < \rho < 0.732$ for octahedral coordination. The lower value indicates the transition to a more stable tetrahedrally coordinated structure and the upper a similar transition to a cubally coordinated structure. Figure 8 shows how poorly the rule holds in practice. Here r_+ and r_- pairs are plotted for a series of AB octet molecules (those containing eight valence electrons). A different symbol is used for each different crystal structure type. Such a plot is called a structure map. The solid lines define the critical radius ratios just described. Out of a total of 98 examples, there are 38 errors, hardly a success rate that encourages confidence in the model. Obvious included in this plot are several systems that are not usually regarded as being "ionic" although in the context of his rules in general Pauling did write[63] "Here ... the use of the word ion is to be interpreted as meaning that the bonds are largely ionic but not necessarily of the extreme ionic type. The bonds in these crystals may have a large amount (50% or even more) of covalent character." However the fact that materials containing very electronegative anions (e.g., O^{2-} or F^-) combined with electropositive cations are incorrectly predicted

TABLE IV. Cell Volumes for Pairs of Isotypic Compounds (Å^3)

NiO	72.4	NiF_2	33.4	NiI_2	88.3
MgO	74.7	MgF_2	32.6	MgI_2	102.1
Fe_2SiO_4	307.9	Fe_2GeS_4	530.7		
Mg_2SiO_4	290.0	Mg_2GeS_4	570.3		

TABLE V. Some Ionic Radii (Å)

	O^{2-}	F^-	Al^{3+}	Na^+
Pauling	1.40	1.36	0.5	0.95
Shannon and Prewitt	1.26	1.19	0.67	1.16

(e.g., BaO, SrO, LiF) suggests that the scheme has some drawbacks.

This is not the place to detail how these radii have been derived. Clearly the sum of an anion and cation radius gives the internuclear separation which of course comes from the crystal structure (r_0 of Figure 7). This may be divided into anion and cation radii in several different ways. Historically a choice was made for the radius of oxygen, since the system-to-system variation in the M–O separation for a given cation coordination number was found to be small. The most recent tabulation of radii, that of Shannon and Prewitt,[64] divides the anion–cation distance by looking at experimentally determined electron densities in solids. It may be argued then that the wrong radius has been chosen in Figure 8. Perhaps we should have chosen the oxide radius differently and used the radii of Pauling rather than those of Shannon and Prewitt. In fact the number of failures of the radius ratio rule is not very sensitive to the actual choice of radii.

There is another problem associated with such "radii" in general. Whereas M–O distances show relatively small variations, M–X linkages, where X is almost any electronegative species other than oxygen or possibly fluorine, show a considerably wider spectrum of distances. The difficulty of constructing a set of self-consistent radii for sulfides, for example, has been discussed at some length.[65] In Table IV we show the cell volumes (in Å^3) for some pairs of isotypic compounds. From these data can it be concluded that Mg^{2+} is larger than Ni^{2+} or that Ge^{4+} is larger than Si^{4+}? Such ambiguity in the definition of a radius means that a scheme such as the radius ratio approach is doomed from the start. Another interesting observation is that the cation radii are somewhat sensitive to coordination number. (We have uniformly used the radii appropriate to six coordination in Figure 8). LiF is predicted to have the six-coordinate rock salt structure if the radius corresponding to four coordination is used but is predicted to have the CsCl structure if the radius for six coordination is chosen! The inescapable conclusion from our discussion is that some of the fundamental axioms of crystal chemistry, now well established in the folklore of the subject, either do not hold up in practice or are too ambiguous to make clearcut choices.

We point out some other problems with the whole traditional "ionic" concept. As mentioned above, the basic approach regards anions as larger than cations. Table V shows the Pauling and Shannon and Prewitt radii for some common ions. In NaF or CaO, for example, this means that instead of having tiny cations sitting in the interstices of an array of large anions, there are packings of ions of roughly equal sizes. Also it is often suggested (and especially so in minerals) that

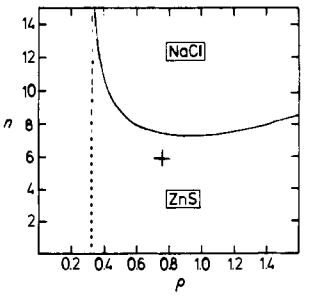

Figure 9. Calculated structural dependence on p and n using an electrostatic model for AB octets. The cross shows the location of LiF. (Adapted from ref 2.)

the volume per O^{2-} ion is constant. This in practice only works for a limited range of systems. In BeO this volume is 13.8 Å^3 and in BaO it is 42.1 Å^3. Finally it is often claimed that many anion packings approximate the close packing of spheres. The close packed density is simply $\pi(\sqrt{2})/6 = 0.740$, but in many systems where the packing is not constrained by symmetry it is sometimes very different. In corundum, for example, the "hcp" packing of spheres gives a packing fraction of 0.595 if all anions are considered of equal size.[41]

What about the theoretical basis of the ionic model so defined? Are the conclusions of Figure 7 applied to local clusters a natural consequence of the electrostatic model applied to the infinite crystal? The answer, perhaps surprisingly is that these local ideas are on rather shaky ground when the model is formulated in the proper mathematical way.[66] Equation 13 gives the ratio of the electrostatic energies of two structures, i, j

$$E_i/E_j = (M_i/M_j)^{n/(n-1)}(Q_j/Q_i)^{1/(n-1)} \qquad (13)$$

where

$$Q_i = m_i + (1.25m_{+i}/\gamma_{+i}^n)(2\rho/(1+\rho))^{n-1} + (0.75m_{-i}/\gamma_{-i}^n)(2/(1+\rho))^{n-1} \qquad (14)$$

An ionic model is used which includes a Madelung constant (M) for each of the two structures to take care of all Coulombic interactions, and repulsive terms between nearest neighbor like and unlike pairs. The latter are characterized by a Born exponent n. If n is very large, then the ions approximate hard spheres. As n gets smaller these spheres get more "squashy". There are m_+ (m_-) cation–cation (anion–anion) nearest neighbor distances at a distance $\gamma_+ r$ ($\gamma_- r$), where r is the anion–cation distance. ρ is the radius ratio and m the coordination number of anions by cations and vice versa.

Figure 9 shows how the lower energy crystal structure depends[66] on the radius ratio ρ and n for the pair of structures ZnS (sphalerite, zincblende) and NaCl (rock salt). As can easily be seen the critical value of ρ of 0.414, which from Figure 7 is supposed to separate four- and six-coordinate structures, has no special significance. In fact for hard spheres a limiting value of ρ = 0.325 is found, the horizontal dashed line on the plot. Similarly, but not shown on the diagram here, the critical value of ρ of 0.732, which from the ideas of Figure 7 separates six- and eight-coordination, has no significance either. In this case the eight-coordinate structure is only found for large and chemically impossible values of n. So the model does not predict any

CsCl structures at all. The general result that smaller cations and softer interactions (smaller value of n) prefer four coordination is in broad agreement with experiment. As an interesting aside Li^+ is found in four-, five-, and six-coordination in mineral structures.

Shown on Figure 9 is a single point, that for LiF, which adopts the rock salt structure. Once again we have a choice of which radii to use in the evaluation of ρ. However, adjustment of the radius ratio can only move points horizontally on the diagram. Notice that the point for LiF can never be moved into the correct (rock salt) region. It has an n value smaller than the smallest value of n which allows the rock salt structure. A similar result leads to the failure to predict any structures with the CsCl structure as we have just noted. These two results cast some serious doubt as to the validity of Pauling's first rule as defined. However in qualitative terms, irrespective of whether the repulsions between the anions are visualized as being electrostatic in origin, supplemented by a generic Born repulsion, or arising via the overlap forces of an orbitally based model, the longer the anion–cation distance the larger the number of anions which can be packed around a given cation. Because oxide minerals make up the largest part of the geological earth, and since metal–oxygen distances, as we mentioned above, show relatively little variation for a given metal, it has proven possible for mineralogists to build a picture of the structures of these materials based upon radius ratio considerations.

We have noted above the implied stability on this basic model of a close-packed array of anions, into which small cations have been placed. Since the anions are charged there is clearly an enormous repulsion between them. The stabilization which prevents explosion of the solid is the strong attraction between anion and cation. This balance led O'Keeffe to suggest[41] that the lowest energy structure is the one which is of maximum volume given a fixed anion–cation distance. Of course such an argument may also be phrased in orbital terms. Anion–cation attractions and anion–anion repulsions are not the sole perogative of electrostatic models. We may use this to cast lights on the geometric details of the rutile structure, **15**, **18**, and **21**.

As we have noted rutile is a tetragonal variant of the orthrhombic $CaCl_2$ type. In the latter the Ca atoms are in 2(a) (0, 0, 0; $^1/_2$, $^1/_2$, $^1/_2$) and the Cl atoms in 4(g) ± (u, v, 0; $u + ^1/_2$, $^1/_2 - v$, $^1/_2$). In rutile $u = v$. The volume of the orthorhombic cell is

$$V^2 = l^6\beta^2(4u + 4\beta^2 v - 1 - \beta^2)/(u^2 + \beta^2 v^2)^3 \quad (15)$$

where l is the anion–cation distance and β is the axial ratio b/a. γ is the axial ratio c/a and is given by

$$\gamma^2 = 4u + 4v\beta^2 - 1 - \beta^2 \quad (16)$$

The maximum volume of the structure from eq 15 occurs at $u = v = 0.300$ (i.e. at the rutile arrangement) and $\gamma = 0.632$ ($\beta = 1$). These numbers should be compared with the observed values of 0.305 and 0.634. Inclusion of O–O repulsions in a more sophisticated way[26] results in a distortion of the rutile structure to give two long and four short M–O distances, as observed. The idea that it is the maximum volume structure which is stable is not always true if one contact is forced by symmetry to be very difficult from the others. Thus although we believe O–O repulsions to be important in determining the structure of anatase (TiO_2), the maximum volume structure gives[26] a Ti–O–Ti angle of 141° compared to the observed one of 156°.

TABLE VI. Cohesive Energies of Some Systems Using the Ionic Model

system	lattice energy, kcal/mol	
	calcd	exptl
NaCl	−180	−184
LiF	−169	−171
AgCl	−187	−219
Li	−154	−188

TABLE VII. Calculated Dimensions of the Rutile Structure (Distances in Å)

	observed	calculated		
		Madelung, plus Ti–O repulsion	Madelung plus Ti–O and O–O potentials	Ti–O and O–O potentials,[a] zero Ti, O charges
a	4.587	4.246	4.593	4.567
c	2.959	3.429	2.958	2.957
c/a	0.645	0.808	0.644	0.647
u[b]	0.305	0.309	0.305	0.302

[a] Adusted to fit the structure. [b] Oxygen z coordinate.

The ionic model has been used for many years to compute the lattice energies of solids. The agreement with experiment is best for system which have large electronegativity differences. For solids such as CdI_2, AgCl, and $HgCl_2$ the agreement is somewhat poorer. The success of such a model in numerical terms has been used to stress the dominance of ionic forces in holding the solid together. However, the lattice energy of LiF is reproduced with about the same accuracy as that for CsF using an ionic model, so there is no clue here as to why the ionic approach fails to predict the correct structure. As an indicator of the dangers associated with drawing conclusions concerning the nature of chemical bonding from the success or failure of numerical calculations based on simple models, we draw attention to the case of lithium metal. Here the cohesive energy (Table VI) is reproduced about as well as that for AgCl (80–85%) if the solids is regarded as being composed of Li^+ and Li^- entities. What is clear is that if the energy of a solid is divided into two parts, one which measures the heat of formation of the lattice from gaseous atoms (the cohesive energy) and a structural part which measures the energy changes associated with a change in crystal structure, the latter is only a few percent of the former. This implies perhaps that one will need to be somewhat more sophisticated when performing calculations aimed at locating the lowest energy structure than when numerically estimating the cohesive energy. There is no doubt that simple ionic type arguments allow a very useful understanding of the relative stability of some quite complex systems. Johnson's monograph,[67] for example, is full of interesting chemistry which follows by imaginative use of the Kapustinskii formulation of the Madelung energy.

Let us return to the point we have just made concerning the dangers of ascertaining the validity of the ionic models from the successful mimicking of the lattice energies. Table VII shows the values of u and c/a for the rutile structure obtained by using several models[68] which simulated the anion–cation and anion–anion potentials in various ways. The first two included a

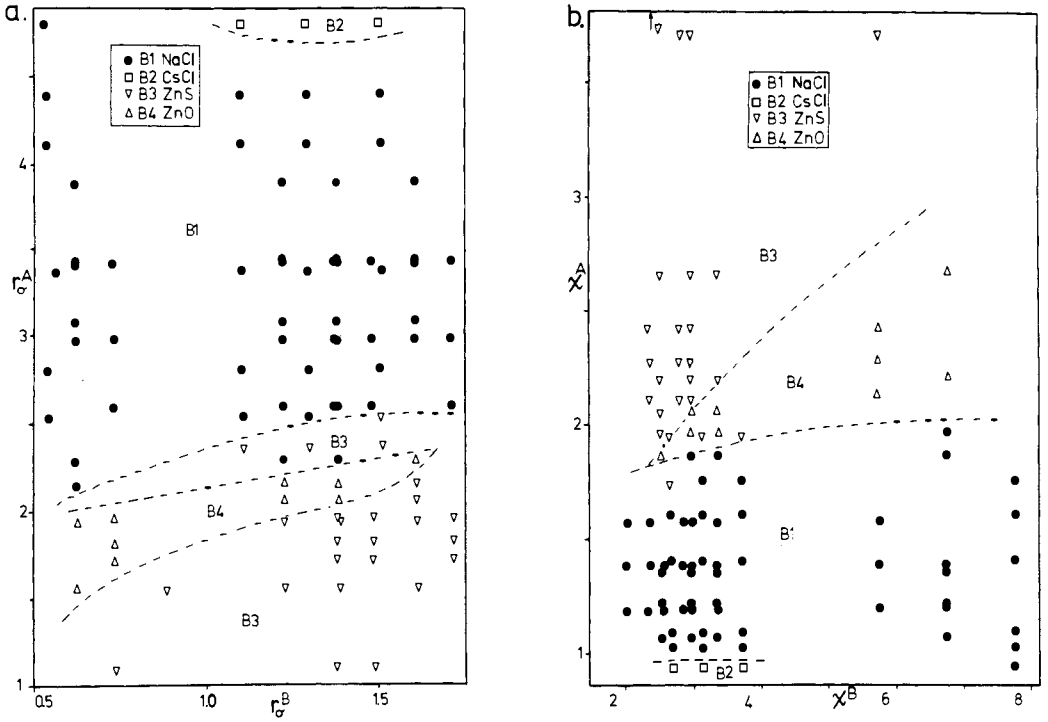

Figure 10. Structure maps for AB octets using pseudopotential radii as indices. (Reprinted with permission from Burdett, J. K.; Price, S. L.; Price, G. D. *Solid State Commun.* 1981, *40*, 923. Copyright 1981 Pergamon Press.)

Madelung contribution (with a charge of +4e on the metal ion) and included an estimate of either the Ti–O or both Ti–O and O–O potentials. (The calculations are then very similar to the MM2 calculations[69] of the organic chemist.) In the third column the results correspond to a set of calculations where the two potentials were adjusted to fit the structure as well as possible. It is particularly interesting to see that the geometry may be successfully modeled for a range of Z values, simply by changing the strength and form of the other potentials. Put another way the geometry may be modeled by using either short range or long range potentials. A similar parallelism exists for SiO_2. Here both an ionic model[70] and a model[71] with parameters for bond stretching and bending from ab initio calculations on small molecules but containing no ionic terms are capable of reproducing the observed structure. As we will see later, the O–O repulsions are important in controlling the details of the structure of rutile.

We have shown some of the problems associated with ionic radii above. However, there is another set of radii, not directly related to them which have shown some promise in crystal chemistry. These are pseudopotential radii[72,73] which are derived as follows. A valence electron feels an attraction for the positively charged nucleus which is strongly screened by the other electrons and increases with decreasing distance. It also feels a strong repulsion which increases with decreasing distance from the nucleus due to the Pauli repulusion forces with the other electrons. The sum of the two gives the pseudopotential, $V(r)$, and the crossing point, the distance at which $V(r) = 0$, is the pseudopotential radius. There are different pseudopotentials of course for s, p, and d electrons (nonlocal potentials) and hence different radii for each value of the l quantum number.

Figure 10 shows structure maps[74] for AB octets using a function of these radii as indices. Here in the left-hand plot we have arbitrarily used the sum $r_\sigma = r_s + r_p$. Since we do not know what the factors are in actually controlling the stability of one crystal structure relative to another, lines are drawn in an arbitrary way so as to separate the examples of one structure type from another. In this sense the approach is a Mendeleyevian one. (We could use the same trick with the ionic radii of Figure 8 of course. The dashed lines on this figure used the same approach.) Notice that the separation of the examples into well-defined regions is extremely good. Addition of ternary stuffed sphalerite or wurtzite examples to the diagram (not shown) also works well. Other maps have been generated which use combinations of these radii as indices.[72,73] In the right-hand plot of Figure 10 we have used the function $\chi = r_s^{-1} + r_p^{-1}$. Since ionization energy scales inversely with the distance of the electron from the nucleus, this function represents a Mulliken electronegativity of some type. In several of these cases the sorting of one structure type from another is perfect. The success of such maps encourages enquiry into why they work. Why is one structure favored over another? This is a tough problem. In molecules where there are extremely good calculational methods for investigating the geometries of molecules and transition states in chemical reactions, one area which is a tough nut to crack is that of molecules containing atoms with different coordination numbers. Usually large CI calculations need to be done. In recent years however Cohen and co-workers have produced some spectacular plots[75,76] of total energy versus volume which not only enabled them to identify the lowest energy structure but also enabled the computation of the transition pressure for moving from one crystal structure to another. Figure 11 shows some results for gallium arsenide. The transition pressure is obtained via the calculated energy and volume changes at the crossing point of the curves. The results are in excellent agreement with experiment. In section IV.E we present a model that is a useful one for un-

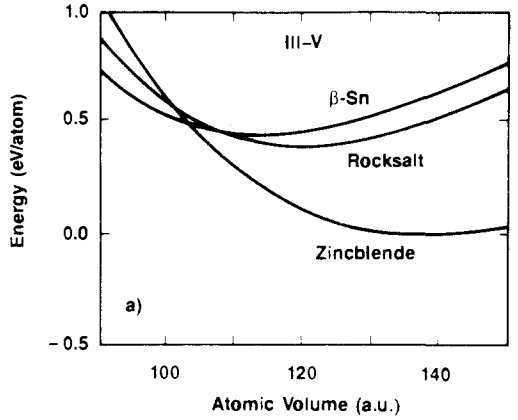

Figure 11. Calculated dependence of structural energy on volume. (Reprinted with permission from ref 113. Copyright 1986, The American Physical Society.)

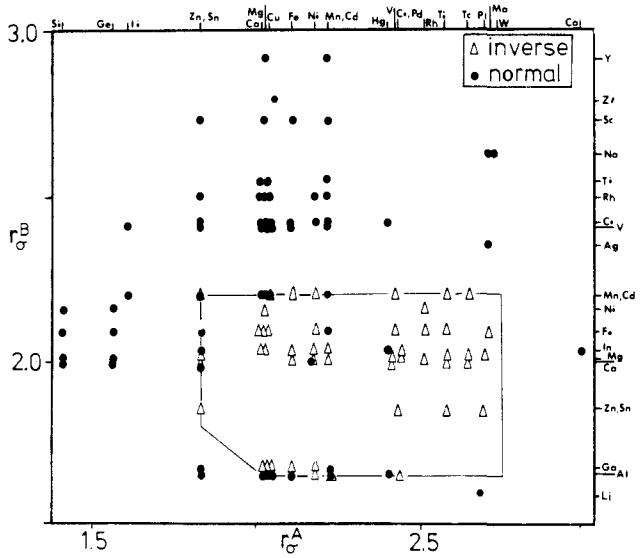

Figure 12. A structure map which sorts normal and inverse spinels. (Reprinted with permission from ref 77. Copyright 1982 The American Chemical Society.)

derstanding a part of this problem.

Figure 12 shows a dramatic sorting of 187 spinel structures into normal and inverse types.[77] The traditional method of understanding whether a spinel is a normal one, $\{A\}[B_2]O_4$, or an inverse one $[A]\{B\}[B]O_4$ where {} and [] represent tetrahedral and octahedral sites, respectively, employs the ideas of a crystal field stabilization energy (CFSE) obtained by seeing how the d-orbital levels of the metal ion split apart in energy in an electrostatic crystal field of negatively charged anions. Nonspherical d orbital populations always have a preference for octahedral over tetrahedral coordination. One of the problems with the approach is that of the 187 spinel examples, only 80 contain at least one nonspherical ion with known spectral (crystal field) parameters so that a prediction can be made. Of this small subset, the ionic approach makes 13 errors. In addition, the thermodynamic consequencies of the CFSE are hugely overestimated.[78] As may be seen from Figure 12, use of the sum of the s plus p pseudopotential radii leads to indices (r_σ) which sort these examples extremely well. There are four errors (two points are coincident) of which two are for poorly characterized examples and may therefore not be errors at all. Notice that along the boundary both normal and inverse types

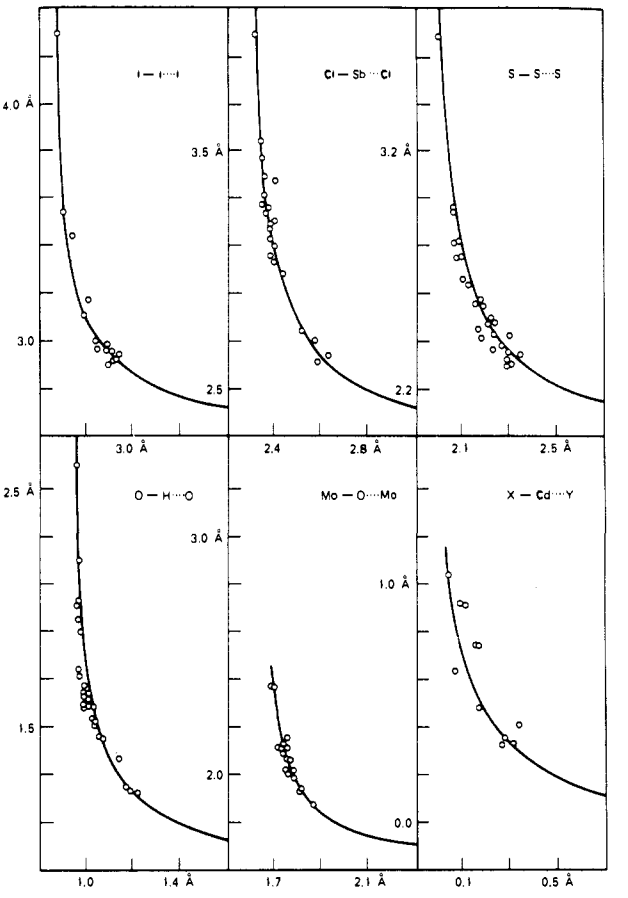

Figure 13. Some structural correlations for the molecules of Figure 14. (Reprinted with permission from ref 58. Copyright 1980 Wiley.)

are found. It is here that the d-orbital-based crystal field arguments come into play and determine the structure. Our conclusion has to be that the major factor determining the structure is similar to that behind the plot of Figure 11 and that the crystal field arguments are only of importance when these forces make no clearcut choice. We will make some more comments concerning the utility of crystal field ideas in section IV in discussions concerning the Jahn–Teller effect.

C. Structural Correlation

One interesting question which is often asked concerning the great collection of structural data that is now available on a wide variety of species is can it be used to cast light on the dynamics of reacting chemical sytems. There is a very useful way which enables a part of the pathway of interacting systems to be plotted out using purely the results of solid-state crystal structure determinations. It is called the technique of structural correlation.[79]

Examination of the spectrum of the internuclear distances found in a crystal structure determination often enables a separation to be made into sets of distances of different type. First, and most obvious, are the close contacts which we often associate with "bonds", the strong interaction holding the system together. The C–Cl distance of 1.77 Å in the CCl_4 molecule is an example of this type. Second, there are the much longer contacts between units, such as the Cl–Cl distance of 3.32 Å in solid chlorine which we assign to

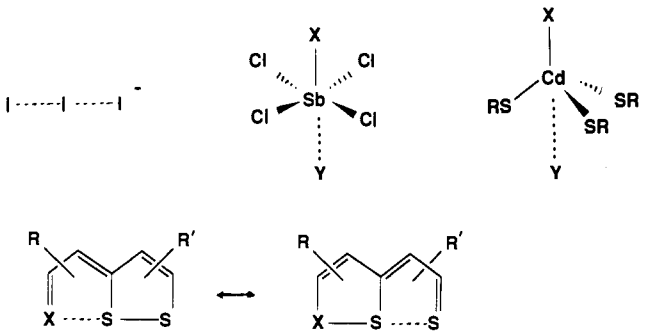

Figure 14. Some of the molecules used in Figure 13.

a nonbonded interaction. This long distance reflects the rather weak van der Waals potential between the atoms concerned. A survey of many systems shows that there are very often a whole collection of intermediate distances which it is difficult to classify as associated with either bonded or nonbonded types. Figure 13 shows some results from crystallographic studies on a series of systems.[80] In the first panel are plotted a set of pairs of I–I distances for solids which contain either I_2 molecules plus I^- ions, or I_3^- ions alone depending upon the assignment of the two I–I distances to bonded or nonbonded interactions. Such an assignment is certainly not clear-cut. The plot shows clearly how one I–I distance (2.67 Å in free I_2) lengthens (to 2.93 Å) in the triiodide ion and the other I–I distance decreases from an obviously nonbonded contact to being bound in triiodide (2.93 Å). Such behavior is qualitatively what we would expect from the bond-valence ideas developed earlier. If the two I–I distances are given by r_1 and r_2, then from the sum rule of eq 3 with eq 1

$$(r_1/r_0)^{-N} + (r_2/r_0)^{-N} = \text{constant} \qquad (17)$$

or

$$r_1^{-N} + r_2^{-N} = \text{constant} \qquad (18)$$

a function which qualitatively describes the behavior of Figure 13. More illustrative in a mathematical sense is the use of eq 2. A little manipulation leads to

$$(r_1 - r_0)(r_2 - r_0) = \text{constant} \qquad (19)$$

which clearly matches the hyperbolic form of this plot.

An interesting question to ask is why the geometries of the I_2/I^- unit are different, i.e. why the same internuclear distances are not found irrespective of the particular crystallographic system. With the presence of different counterions, the unit must experience a different local potential and as a result distorts along the distortion coordinate with a low lying valley. Also shown in Figure 13 are similar plots for the systems shown in Figure 14 along with some hydrogen bonds and data from molybdenum oxides. They nicely show geometrically how bonds are made and broken. The last plot shows the transition state for the S_N2 process for nucleophilic attack at tetrahedral Cd. We may use angles as indices too in such diagrams. Figure 15 shows the correlation between angle and distance for another well-studied chemical process, that of the S_N1 reaction. The indices are defined in Figure 16. Here we collect data from crystal structures for that set of tetrahedral PO_4, SO_4, XSO_3, and $XSnCl_3$ units which have local C_{3v} symmetry. The data show very nicely how the geometries of MX_3 and MX_3Y units are connected in textbook fashion. They have been plotted in a special way however. Via the obvious scaling parameter (r_0) in eq 2, we can define a new index $\Delta r_i = r_i - r_{0i}$. Thus Figure 15 shows a composite plot[80] for the SO_4, PO_4, etc., units. The general form of these plots may be understood by using simple bonding ideas concerning the strengths of hybrid orbitals of various sorts or, more quantitatively,[81] by using the simple orbital ideas of the angular overlap model. Figure 16 shows the relationship between the bond angles and the difference (Δ) in the molecular orbital stabilization energy using this model.

We may use this technique to investigate an inorganic example, that of the pathway linking square-pyramidal and trigonal-bipyramidal low-spin d^8 and d^9 molecules.[81] In Figure 17 $\theta = 60°$ corresponds to the trigonal bipyramid and $\theta = 90°$ the square pyramid. Plotted are

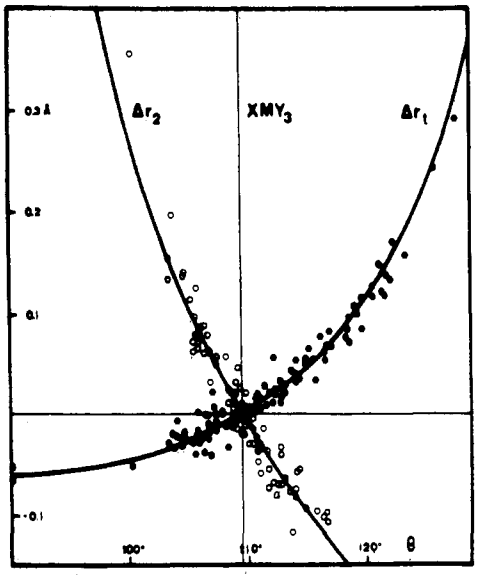

Figure 15. Structural correlation for an S_N2 process. (Reprinted with permission from ref 79. Copyright 1975 VCH Publishers.)

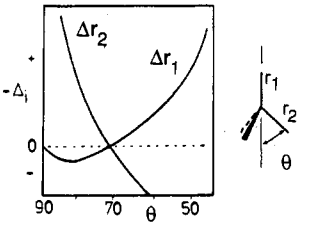

Figure 16. Plot of molecular orbital stabilization energy against θ for S_N1 reactions. (Reprinted with permission from ref 81. Copyright 1979 The American Chemical Society.)

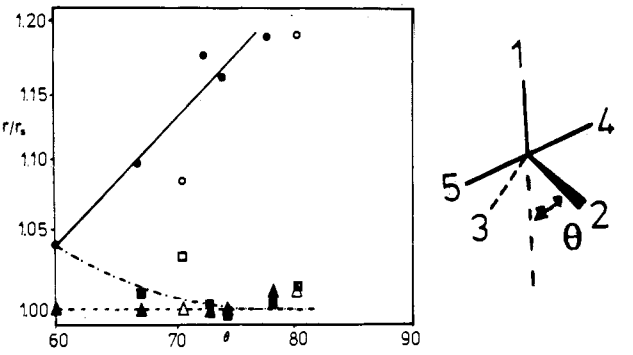

Figure 17. Structural correlation plot for the square pyramidal to trigonal bipyramidal conversion. See text for details. (Reprinted with permission from ref 81. Copyright 1979 The American Chemical Society.)

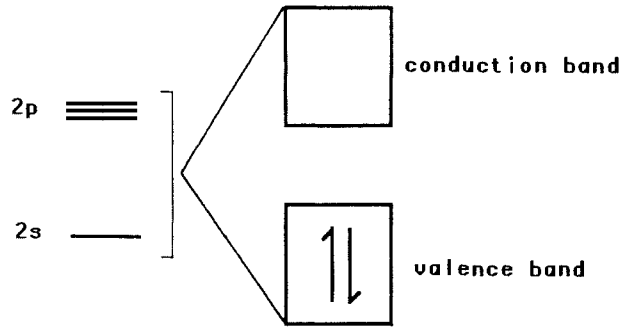

Figure 18. Schematic generation of the band structure of diamond.

the geometrical data[82] for $CuCl_5^{3-}$ (solid symbols) and $Ni(CN)_5^{3-}$ (open symbols). Circles, squares, and triangles represent, respectively, the values for r_1, the average value of r_2 and r_3, and the average value of r_4 and r_5. r/r_s represents a normalized bond length parameters. It is the ratio of a given bond length to the average value found for r_4 and r_5 in the trigonal-bipyramidal geometry or the geometry closest to it. Results such as these give interesting insight into subsitution reactions at square-planar MX_4 systems, for example, and are approachable by simple orbital ideas.[81,83]

IV. Some Electronic Structure Problems

A. Localized and Delocalized Bonding

The models we have used so far have avoided the explicit use of electron energy bands. In solids, just as in molecules, there is competition between use of localized and delocalized models to describe their chemical bonding. As long as there are two electrons which may be assigned to a chemical bond between two atoms, the localized picture, with its ties to the ideas of G. N. Lewis, is a possible one. The delocalized picture is usually more complex.[25] It can of course be used to look at the bonding picture in molecules where the localized picture is applicable (and in fact must be used if we are interested in spectroscopic problems) but is the only real way to describe, for example, the π-manifold of planar aromatic hydrocarbons and the three-dimensional aromaticity of inorganic cage and cluster molecules.[25] In CH_4 we have a choice of models, either a localized picture can be used (four two-center, two-electron bonds) or a delocalized one (occupied t_2 and a_{1g} bonding orbitals). The localized orbitals are constructed in a straightforward way from the occupied delocalized ones. There are exactly four bonding occupied bonding delocalized orbitals in CH_4 which may be used to form the four equivalent localized C–H bonding orbitals. In SF_6 we have no choice. There are only four occupied delocalized bonding orbitals (there is a degenerate lone pair orbital) and six "close contacts". Three-center, delocalized, bonding along all three Cartesian directions must be used. So the S–F bond order is $^2/_3$. Forcing the involvement of d orbitals to produce six d^2sp^3 hybrids is artificial, and an approach we will reject. The extent of d orbital involvement is small. Neither would we envisage the use of dsp^3 hybrids in well-characterized five-coordinate carbon systems,[84] since this is a first-row element.

In solids an analogous situation applies. In a material such as diamond, the electronic situation is well-described by an energy band picture assembled from the valence s and p orbitals on the carbon atoms as shown in Figure 18. These bands may be generated by using tight-binding theory, the solid-state analogue of the molecular chemists LCAO method.[1,85] With four electrons per atom the lower energy band is full and diamond is an insulator. The organic chemist however, uses localized hybrid orbitals to describe all three species 1–3. This is a perfectly valid approach too. There are exactly the same number of electron pairs in this occupied band as there are "bonds" in the solid and so localized orbitals may readily be constructed from these delocalized crystal orbitals. Similarly in all the polymorphs of SiO_2 which contain four-coordinate silicon, localized two-center two-electron bonds between silicon and oxygen may be readily visualized. However an energy band picture may be readily constructed for this material, where there are exactly the same number of doubly occupied Si–O bonding crystal orbitals as there are "bonds". In LiF, which has the rock salt structure, the situation is analogous to that for SF_6. There are six close contacts around each atom and only four pairs of electrons. The energy band picture will look similar to that for diamond. There is a gap between the highest occupied (containing eight electrons per formula unit and being largely fluorine located) and lowest unoccupied (largely lithium located) bands requiring this material to be an insulator, which it is. However now we have to describe the bonding picture in terms of a delocalized picture, where the crystal orbitals run through the whole crystal. Clearly for this species it would be ludicrous to insist on the provision of d^2sp^3 hybrid orbitals at each site. Also there are only four electron pairs to make bonds. With the delocalized approach the bond order is $^2/_3$, just as in SF_6.

SCHEME II

8 electrons		9 electrons		10 electrons
NaCl (rock salt)		→		GeTe (arseniclike)
ZnS (wurtzite)	→	GaS (slab structure)	→	GeTe
BN (graphitelike)		→		GeTe

Our choice of model makes no commitment to the electrical properties of the material. We have to use the delocalized model in LiF but it is certainly not a metal. In both graphite and stishovite (SiO_2 in the rutile structure containing six-coordinate silicon) the delocalized picture has to be used too. But graphite, where an energy band is only partly full, is a metal (although not a very good one), and stishovite, where the band occupancy is similar to that in Figure 18, is an insulator.

The dependence of molecular electronic structure on electron count is well known. The change in angular geometry along the series BF_3, NF_3, and ClF_3 on moving from a six-electron to ten-electron species has been long understood. Sometimes as the electron count increases, antibonding orbitals are occupied, and an increasing number of linkages of a parent structures are broken. For example[86,87] the P_4 tetrahedron has a total of 20 electrons and six P–P linkages, B_4H_{10} has two more electrons and five close B-B distance, $P_4(CF_3)_4$ has 24 electrons and four P–P linkages, and, finally, PCl_3 has

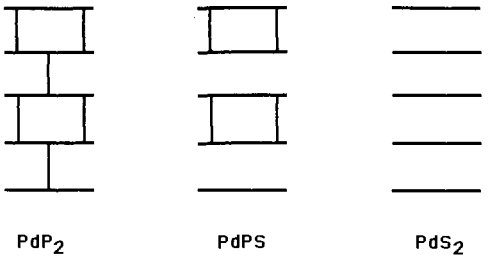

Figure 19. Schematic showing the breakup of the PdP_2 structure to that of PdS_2. (Two of the sheets are shown in **31**.)

26 electrons and three bonds. Scheme II shows a similar scheme[87] for understanding the relationships between the structures of some simple solids. All three systems end up at the puckered 6^3 sheet structure of GeTe which is a derivative structure of elemental arsenic and antimony. We may get there either by breaking the linkages of six (NaCl) or four (wurtzite) coordinate parent structures or by pucking the graphite-like layer structure of BN. The first of these is shown in an idealized form, in **30**, along with an alternative bond-

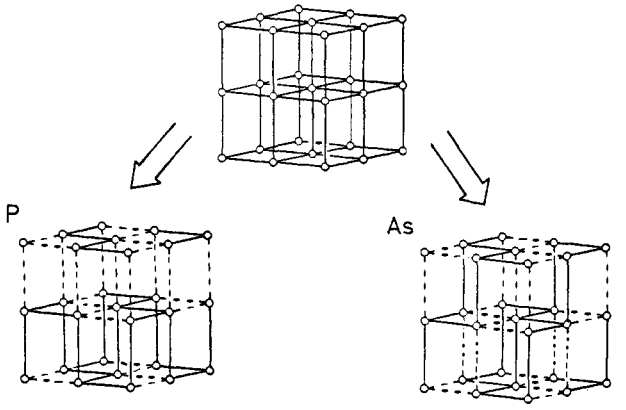

30

breaking pattern which leads to the net found in black phosphorus. Each step occurs as a result of the increase in electron count. Figure 19 shows another example[88] of the same type. These are from the Pd/S/P system. the basic building block is shown by a solid line in this diagram. It is a puckered $5^4 + 5^3$ (2:3) net containing these elements. In PdPS (21 electrons) each adjacent pair of sheets are linked via P–P bonds (there are no S–S interactions between these sheets) to give a two-dimensional slab structure. Structure **31** shows the two

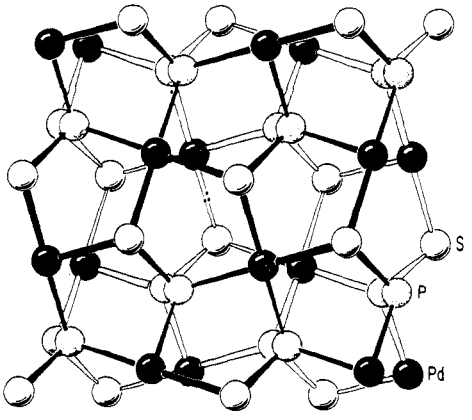

31

sheets of one of these slabs from above. The phosphorus atoms are the mottled open circles and the metal

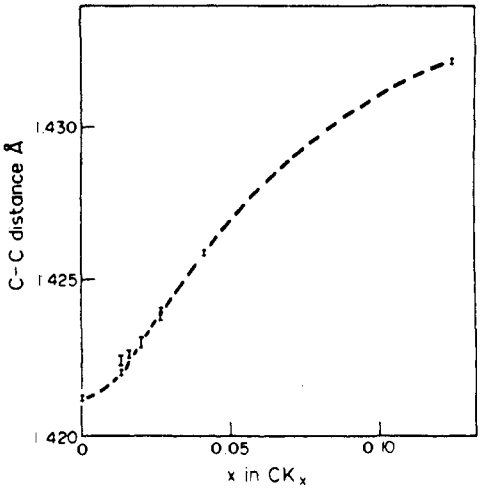

Figure 20. Dependence of C–C distance in graphite on concentration of potassium intercalant. (Adapted from ref 90.)

atoms the closed ones. There are no P–P linkages between the slabs. In PdP_2 with 20 electrons there is a three-dimensional network of P–P linkages. In PdS_2 with 22 electrons there are no S–S interactions at all between the sheets. The structure is of the pyrite type, with a strong octahedral → square distortion about the metal center as expected for the d^8 metal. As a result there are only weak forces between the sheets. Simple electron counting in all of these examples of course enables us to readily identify the number of two-electron bonds and lone pairs present, and so how each of the structures is put together is easy to see. It is the geometrical relationships between them which are interesting.

Not always of course does the addition of electrons give rise to a dramatic structural change. If the extra electrons fill nonbonding levels, the result may be rather tiny. There are cases too where addition of electrons to antibonding levels leads to no change in structure. For example, in molecular transition-metal complexes of stoichiometry MX_6 the addition of electrons to the e_g orbitals, which are metal–ligand σ antibonding, leads to a lengthening, but generally not a fission of the bond. In the AlB_2 structure, found for many first-row transition metal borides MB_2, there is no dramatic structural change on moving from M = Sc to M = Mn, just a gradual lengthening of the M–B distance.[89] Figure 20 shows how the C–C distance in graphite varies with the extent of intercalation by potassium.[90] Since the orbitals in graphite which are being filled by the additional electrons are antibonding between adjacent carbon atoms, the lattice gradually expands with addition of alkali metal.

B. Ordering Patterns of Atoms in a Lattice

One aspect of structural chemistry of fundamental importance is one which we will call the coloring problem.[91] Consider a fixed molecular or solid-state framework (e.g., a square or the hcp lattice) which is then populated with different sorts of atoms or atom groupings. Such a mapping of vertices to atoms is called a coloring, and the different atoms or units are associated with different colors. We require exactly one atom or atom grouping to lie at each vertex in the

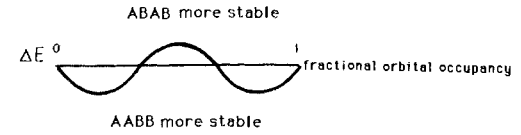

Figure 21. Expected dependence of stable structure on electron count for "coloring" problems of the type described in the text.

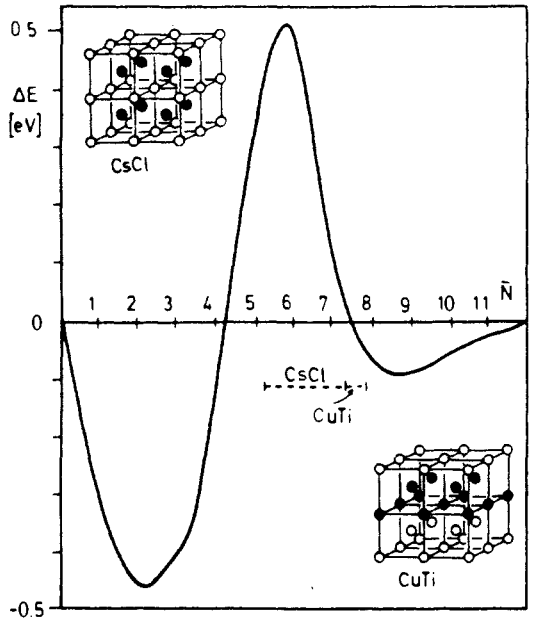

Figure 22. Calculated energy difference curve between CsCl and CuTi structures for transition metal alloys as a function of average number of (s + d) electrons. (Reprinted with permission from ref 91. Copyright 1985 The American Chemical Society.)

framework. In addition we require the coloring to maintain a specific stoichiometry.

Examples of the problem are given in structures **32** and **33**, the square and the bcc lattice. Their stoi-

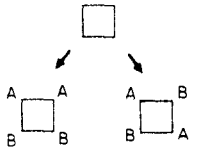

32

chiometries are A_2B_2 and AB. One of stoichiometry AB_2 might be the coloring of the triatomic molecule Br_3^- to give $ClBr_2^-$. Many other examples immediately spring to mind. The rock salt structure, for example, is an AB coloring of the simple cubic lattice. We shall make use

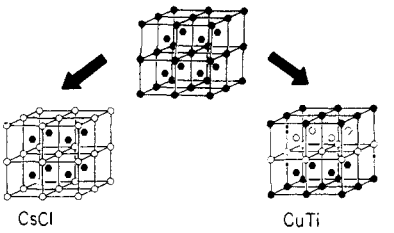

33

of this description later. There are only two possible colorings for **32** but an infinite number for the extended solid-state arrays of **33**. For a unit of finite size, however, the number of possible colorings is finite.

A question which often interests chemists is which coloring has the lowest energy. A method which may be used here to make progress with this problem is the method of moments.[92,93] Instead of considering the energies of a set of electronic levels, $\{\epsilon_i\}$, for a molecular or solid-state structure we describe the level structure in terms of moments, $\mu_n = \sum_i \epsilon_i^n$. These moments may be directly related to geometrical features of the structure. If two structures differ first at the nth moment, then the energy difference curve between them as a function of band filling very often has a very characteristic shape which is determined by the value of n. The coloring problems shown in **32** and **33** are determined by the fourth moment curve shown in Figure 21. The point $x = 0$ corresponds to the case of the completely empty band or collection of orbitals; $x = 1$ corresponds to the full band. Carbon chemistry with a s^2p^2 configuration corresponds to $x = {}^1/_2$.

The curve tells us that at the half-filled point the alternate pattern ...ABAB... is preferred, but at the quarter and three-quarter positions the adjacent ... AABB... pattern is favored. Notice that in the cyclobutadiene case in **32** the coloring on moving around the ring may be described in these terms. For the bcc lattice **33**, notice that the coloring of adjacent planes of atoms may be described similarly. Cyclobutadiene itself has a half-filled $p\pi$ band. (There are four carbon $p\pi$ orbitals each containing one electron.) Theory predicts the stability of the ABAB pattern for this electron count. Indeed all "push–pull" cyclobutadienes (e.g. $C_4[N(C_2H_5)_2]_2[COOC_2H_5]_2$) and molecules of the type $B_2P_2R_4$ have this arrangement.

Figure 22 shows the calculated energy different curve[94] for two transition metal–transition metal alloy structures, CsCl and γ-CuTi, derived from the bcc lattice (**33**). Compare the shape of the computed curve with that of Figure 21. Notice how the computed curve

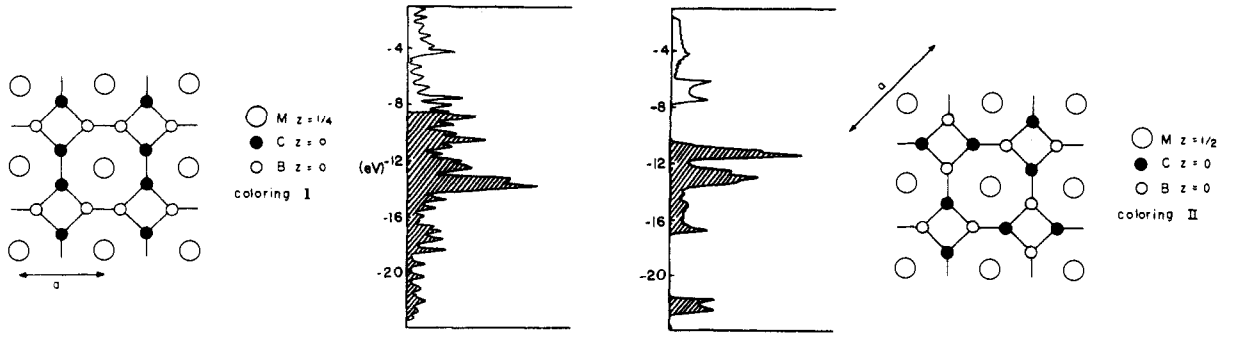

Figure 23. Electronic densities of states and coloring patterns in $M_2B_2C_2$. (Reprinted with permission from ref 95. Copyright 1986 The American Chemical Society.)

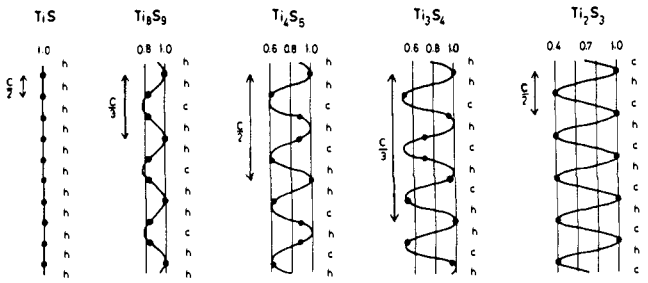

Figure 24. Occupancy wave and nature of anion packing in the titanium sulfides. (Reprinted with permission from ref 97. Copyright 1970 Academic Press.)

nicely separates known examples of the two types, shown by a dashed line on the plot.

The ordering of the atoms over a lattice can dramatically alter the properties of the system. In Figure 23 are shown two of the possibilities for the CaB_2C_2 structure. This consists of 48^2 nets of atoms (polymerized squares) between which lie metal atoms. Also shown are the corresponding calculated densities of states.[95] It is obvious that even the general appearance of the density of states depends markedly on the ordering pattern. As a result one of the materials is predicted to be an insulator (or perhaps a semiconductor) while the other is a metal. The theoretical result is that the insulating possibility is more stable. The crystallographical results are not yet firm but the tentative suggestion is that coloring I best satisfies the diffraction results.[96] No electrical measurements have been reported which would have helped sort out this problem.

Figure 24 shows the experimentally determined[97] ordering patterns of the Ti atoms in the series of sulfides TiS_x. The numbers show the fractional occupancy of the octahedral holes between each pair of close-packed layers. Notice the very striking feature of an "occupation wave" and how the manner of stacking the close-packed planes of sulfur atoms depends upon the chemical composition. Similar, rather specific ordering patterns are found for several other sulfides of this type. At present we do not have an explanation for this fascinating ordering of the metal atoms or the packing of the sheets.

In section II.C we showed two different ways of ordering the ions over a hexagonal eutactic array to give the rutile (**15**) and α-PbO_2 (**16**) structures. This also turns out[98] to be a fourth moment problem, associated this time with through space interactions between the σ-nonbonding "t_{2g}" set of metal d orbitals. Figure 25 shows calculated energy difference curves between the two structures as a function of d count using tight-binding theory. Their shape is broadly in agreement with the experiment. For transition-metal dioxides the α-PbO_2 type is only found for ReO_2, a d^3 system. This electron count exactly half-fills the "t_{2g}" band. The top curve is for the undistorted rutile structure with equal metal–metal distances, the bottom for the MoO_2 variant where the metal–metal distance alternates in length along the chain.

The shape of the curve may be understood by making connections with small molecule chemistry.[93] At the half-filled point the most stable computed structure from Figure 25 is (α-PbO_2) the one where (approximately) each of the two potent d orbitals on the metal

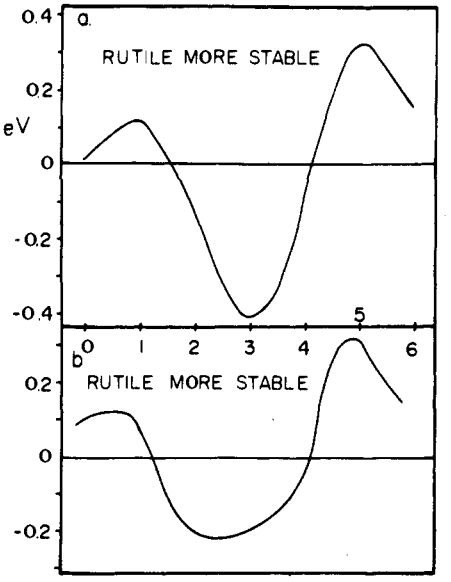

Figure 25. Calculated energy difference curves for the rutile and α-PbO_2 structures. See text for details. (Adapted from ref 98.)

is involved in a single interaction with one of its neighbors (**34**). At the quarter and three-quarter filled

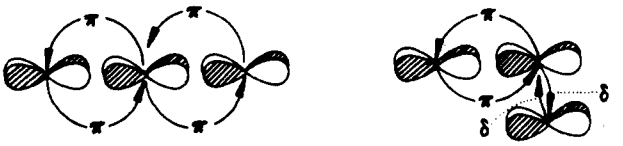

34 **35**

points it is the structure (rutile) where one orbital is involved in strong interactions with both neighbors (**35**) which is more stable. The stable D_{2d} structure of allene, where the π orbital on each CH_2 unit overlaps with a different central atom π orbital, is then the analogue of the α-PbO_2 structure. The planar allene type structure, where only one central atom π orbital is used, is calculated[99] to be stable for a smaller electron count corresponding to the quarter-filled point on the diagram. Such ordering problems are important in understanding the origin of the basic differences between the stability of geometrically rather similar structures.

C. Structural Differences between Solids Containing First- and Second-Row Atoms

One of the striking points concerning the crystal structures of AB_2 compounds is that for six-coordinated cations the rutile structure (**21**) is invariable found for B = O, F but one of the cadmium halide structures (**22**) is found for the cases where B is a second-row or heavier element. How may we understand this? Clearly the cations locally have an octahedral geometry in the ideal form of both of these structures which means that the geometric preferences of the anion bear examination. In the rutile structure the anion is planar, but in the cadmium halide structure it is pyramidal. In many early-transition-metal oxides there are also planar oxygen coordination environments. The anatase and hollandite types are two examples. In the structures of TiO and NbO a very unusual square-planar oxygen coordination is found.[100] Pyramidal oxide geometries are found too, but not for any binary system. $NaFeO_2$ has a stuffed cadmium iodide structure, but here the

anion is coordinated, not only by the Fe atoms which make up the layers but by the stuffing Na atoms.[101] (This is then a superstructure of rock salt.) Similar structures are found for Li_xMoO_2 and Na_xMoO_2. Recall that use of a model which simply maximized the volume of the structure subject to a fixed anion–cation distance led to a planar geometry at oxygen for the rutile arrangement, but is there an electronic effect too? An excursion into main group chemistry is useful here.

If the anion geometry is important we need to ask how the pyramidality of an AX_n species can be controlled?[25] $N(SiH_3)_3$ has a planar skeleton, but the phosphorus analogue $P(SiH_3)_3$ is pyramidal with a Si–P–Si angle of around 96°. The molecule $N(CH_3)_3$ is nonplanar too. Planar nitrogen is found in the solid-state structure of Ge_3N_4 and planar carbon in the ion $C(CN)_3^-$. In all of these cases electron counting would have predicted a pyramidal structure just as in ammonia. The square-planar oxygen geometry in NbO is without parallel in molecular chemistry. Planar geometries at phosphorus are only known in transition-metal complexes. **36** shows electronically how we believe this

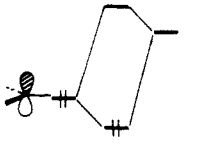

36

occurs.[25,98] If the ligands have available, low lying, empty acceptor orbitals of π type, then they may overlap with the central atom p orbital (the HOMO of the unit) and stabilize the planar structure. In SiH_3 these orbitals are the Si–H σ^* levels, in CN they are the π^* levels as shown in **37**. In molecular organic chem-

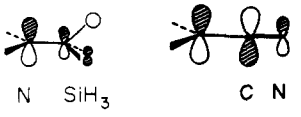

37

istry there is a very similar effect (the anomeric effect[102]) which is understandable using the same idea. **38** shows how an oxygen lone pair orbital may be sta-

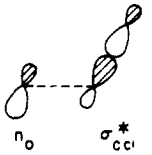

38

bilized by overlap with a C–X antibonding orbital (just like the antibonding Si–H orbital above). The result is a strengthening of the C–O bond and a weakening of the C–X bond. **38** shows a conformationally locked

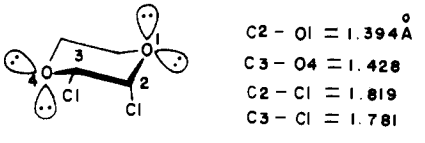

cis-2,3-dichloro-1,4-dioxane

39

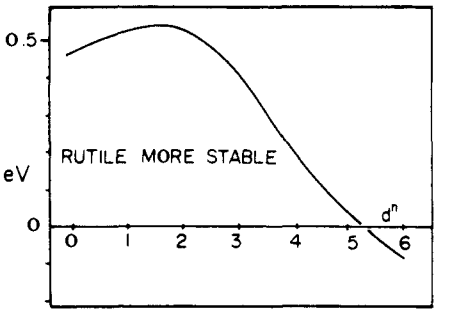

Figure 26. Calculated energy difference curve for the rutile and $CaCl_2$ structure types. (Reprinted with permission from ref 98. Copyright 1985 The American Chemical Society.)

1,3-dioxane where one of the O–C–Cl units (O1–C2–Cl) is oriented in just the right way for such an interaction, while the other is locked in a geometry where such an interaction may not occur. Notice the shorter C2–O1 bond compared to C3–O4, and the longer C2–Cl distance compared to C3–Cl. In TiO_2 and NbO an exactly analogous stabilization by the empty metal π-type orbitals of the t_{2g} block may occur as in **40**. A calculation[103] ascribes ~13 kcal/mol to this type of interaction for the Ti–O case. In the two-coordinate situation we believe that it is an interaction of this type which leads to the very soft bending potential at the oxygen atom described in section IIB. Here there are only two acceptor orbitals to overlap with the relevant oxygen p orbital, and the result is not always large enough to force a linear geometry. (Linear Si–O–Si structure are known, one example being in the mineral coesite.[104])

If the mechanism shown in **40** is a good one, why are

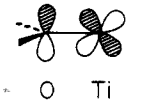

40

planar geometries rarely found for second-row and heavier atoms? The answer lies in the much stiffer σ framework in, for example, PH_3 compared to NH_3 or in H_2S compared to H_2O. For the former pair of molecules the inversion barrier is about 5 kcal/mol in NH_3 and some 35 kcal/mol in PH_3. Thus the acceptor effect needs to be much stronger for phosphorus compared to nitrogen in order to force a planar structure. Consequently there are fewer examples and MX_2 compounds with heavier than first-row X atoms either have the cadmium halide structure, the molybdenite or a related arrangement, or perhaps one of the zirconium halide structures, each of which contain pyramidal nonmetal atoms.

We also mentioned in section IIB another model which leads to similar results in terms of nonbonded repulsions between the silicon atoms or between the cations in general. Certainly these forces are present, but how important are they in determining these structural features? There is one prediction that the electronic π-bonding model makes which may be used to test out its validity. As the metal t_{2g} set is filled with electrons, the driving force for the planar structure will decrease.[98] With reference to **36**, for a d^0 metal the interaction is a stabilizing two-orbital, two-electron one, but in a d^6 metal it has become a destabilizing two-orbital, four-electron one since now the upper orbital

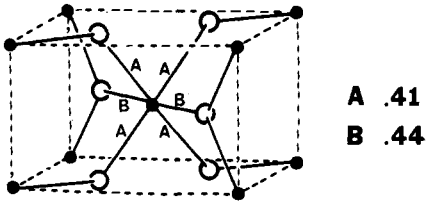

Figure 27. Computed band overlap populations for rutile. (Reprinted with permission from ref 98. Copyright 1985 The American Chemical Society.)

is full. Recall that the $CaCl_2$ structure is a rutile variant with a pyramidal anion geometry. Figure 26 shows a computed energy difference curve for the two structures, rutile and $CaCl_2$, as a function of d count. Notice the crossover in stability just before the d^6 point. In nice agreement with our model, PtO_2 with this electron count is known in the $CaCl_2$ structure.

But let us pursue the electronic model further. Figure 27 shows the calculated bond overlap populations from a tight-binding calculation[98] for the idealized rutile structure where all of the Ti–O distances are set equal. The prediction to be made from this result is that on electronic grounds from consideration of these nearest-neighbor interactions only, two short and four long Ti–O distances are to be expected in the "real" structure. This is the converse of what is found in rutile TiO_2, but is in fact the correct geometry in rutile MgF_2. We showed earlier that the local geometry in rutile could be matched by choice of a suitable O–O potential. If the O–O distance is short, then these O–O interactions are important. In the fluorides, not only are the M–F distances larger than in the oxides, but the fluoride ion is "smaller". (By which we mean that for a given internuclear separation F–F repulsions are smaller than O–O repulsions.) The picture that then emerges concerning the geometric details of the rutile structure is that it is set by the balance between attractive M–X forces, where π bonding plays a key rôle, and repulsive forces between the anions. In orbital terms we consider these steric effects as arising via the overlap of closed shells of electrons. In rutile itself the strong interactions between anion and cation give rise to short Ti–O and therefore short O–O distances. The strong anion–anion repulsions that these close distances create control the local geometry about the metal (two long and four short Ti–O distances). In the fluorides where these interactions are less important, the M–F distances are set by the anion–cation interactions represented in Figure 27. In MgF_2 for example there are two short and four long Mg–F distances. The anion coordination geometry is controlled by both electronic (the π-bonding of 40) and repulsive anionic contributions. In the fluorides with the rutile structure the electronic component is expected to be smaller than in the oxides on simple electronegativity grounds. In fact there is no changeover in structure with d count in the series as is predicted for the oxides in Figure 26. All of these fluorides have the rutile structure, or its monoclinically distorted variant (for CrF_2 and CuF_2) as a result of a Jahn–Teller distortion (vide infra).

In this section, not only have we illustrated the differences between solids containing elements from different rows of the periodic table, but we have pointed out some of the reasons for the structural differences between isoelectronic oxides and fluorides. We will elaborate further on these below.

TABLE VIII. Local Coordination in Transition-Metal Oxides and Fluorides (Distances in Å)

system	4 linkages at	2 linkages at	difference	distortion type
MgF_2	1.998	1.979	–0.02	B
CrF_2	2.01[a]	2.43	+0.43	A
	1.98			
MnF_2	2.131	2.104	–0.03	B
FeF_2	2.118	1.998	–0.13	B
CoF_2	2.049	2.027	–0.01	B
NiF_2	2.022	1.981	–0.03	B
CuF_2	1.93	2.27	+0.34	A
ZnF_2	2.046	2.012	–0.03	B
TiO_2	1.945	1.986	+0.03	A
CrO_2	1.9112	1.8878	–0.02	B
RuO_2	1.984	1.942	–0.04	B
OsO_2	2.006	1.962	–0.04	B

[a] Monoclinic structure. Three pairs of distances.

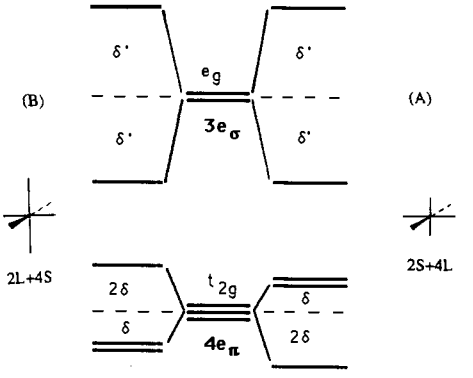

Figure 28. Energy splitting pattern on distortion of an octahedral complex.

D. The Jahn–Teller Effect

Many of the textbook examples of the Jahn–Teller effect are from the chemistry of extended arrays. We shall show here, by using the rutile structure of the previous section, that the electronic situation is really rather different than that usually presented. Not only are the electronic requirements of the local MX_6 geometry important,[105] but so are the extended interactions within the solid. The rutile structure for TiO_2 contains two long (L) and four short (S) Ti–O distances. Since this corresponds to a d^0 configuration, this distortion cannot be due to a Jahn–Teller effect, and as we have described above and in section IIB, it is controlled by nonbonded interactions between the oxide ions. Shown in Table VIII are the details of the metal coordination in all known rutile-type transition-metal oxides and fluorides. Examples of both type of distortion, namely two short/four long and two long/four short are found. Figure 28 shows how the d levels split apart on distortion via these two distortion modes for an isolated MX_6 unit. The energetics of the distortion are controlled by the magnitude of σ and π bonding to the metal for cases involving e_g and t_{2g} degeneracies, respectively. We have used the angular overlap model here and the changes in magnitude of the e_λ on distortion are given by δ and δ'. The use of the angular overlap model[61] or the corresponding approach using the simple ideas of crystal field theory do not give any clues as to the form of the distortion that the Jahn–Teller theorem predicts for the case where an e_g de-

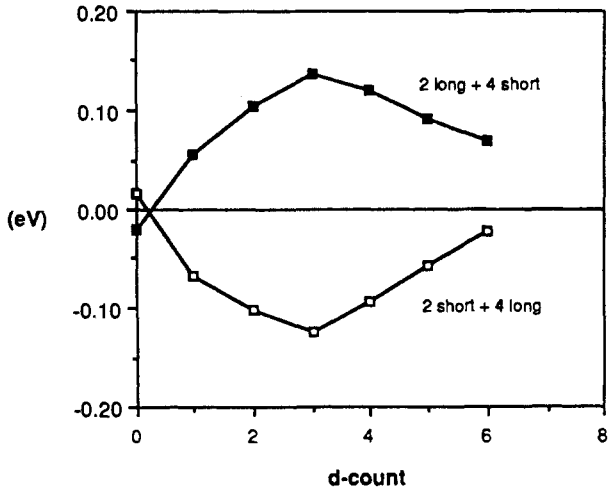

Figure 29. Calculated energy difference curves for two distortions away from octahedral for the rutile structure.

generacy is encountered in this isolated molecular case. Inclusion of s–d mixing into the orbital model via a second-order Jahn–Teller interaction however does allow a rationalization[105] of the virtually universally observed distortion mode (type A). Both of these simple models do make predictions however, for the cases where there is a t_{2g} degeneracy. With reference to Figure 28 we can see that for a d^1 or low-spin d^2 metal two short and four long distances are predicted. For high-spin d^2, low-spin d^4 etc., the opposite is predicted, two long and four short distances should be found.

For two of the fluorides (Cr and Cu) the distortions are locally of the same type as in TiO_2. (They are actually more extreme, and give rise to a monoclinic distortion of the teragonal rutile structure.) These are the classic cases of Jahn–Teller distortions associated with an orbital degeneracy in σ-antibonding orbitals. Notice that the opposite direction of the octahedron to give two short and four long distances is often found. The size of this distortion is usually similar in size to that found for the d^0 species MgF_2. FeF_2 is an exception. It has an orbital degeneracy associated with the t_{2g} orbital set. The distortion associated with this species is exactly as would be expected from Figure 28, but why is no distortion of the opposite type found for CoF_2? A similar result is found for the oxides, where we have already underlined the importance of π bonding. From Table VIII it is obvious that some of these distortions are in the opposite sense to what would be expected from Figure 28. Specifically, the dioxides of Cr (high-spin d^2) and Os and Ru (low-spin d^4) have two short distances, whereas two long would have been predicted. For the high temperature form of VO_2 these ideas would have predicted a distortion of type B, but type A is actually found.

These structural results may be put into perspective by looking at the extended array.[106] Figure 29 shows a calculated energy difference curve for a transition-metal dioxide for the two types of distortion. The curve was constructed from a band structure calculation on the infinite solid dioxide. Notice that it implies two regions of behavior in the "t_{2g}" block. For d^0 systems it predicts two long and four short distances. This, as we have mentioned is a distortion controlled by O–O nonbonded forces. For d^1–d^6 it predicts two short and four long distances. This is in quite good agreement

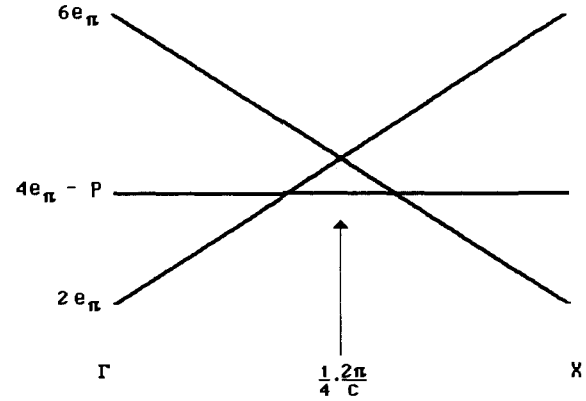

Figure 30. Schematic band structure of the "t_{2g}" orbitals of a one-dimensional rutile chain, showing the stabilization of one component by mixing with one component of the "e_g" orbitals.

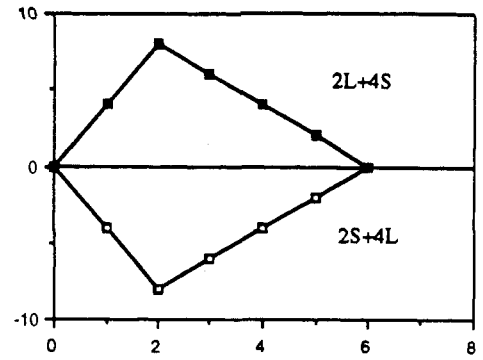

Figure 31. Calculated energy difference curve for the same distortions as Figure 29 using the angular overlap model for a 1-D chain.

with experiment. Notice that there is no stabilization of type A for any occupancy of the "t_{2g}" block.

The form of this energy difference curve is very interesting indeed. It tells us that we may not use the local ideas of the crystal field theory to really understand the distortion mechanisms in these systems but must use an orbital model which takes into account the translational periodicity of the material. We can readily discover the reasons behind the form of this energy difference curve. Figure 30 shows in schematic form the energetic behavior with wavevector (the dispersion) of the "t_{2g}" levels for a single one-dimensional chain of edge-linked octahedra torn from the rutile arrangement of 18. The energy levels are expressed in terms of the parameters of the angular overlap model and show the behavior in the one-dimensional Brillouin zone. The energy evaluated at the mean value point $(1/4)(2\pi/c)$ should be an approximation to the total energy of the system. An important feature of the extended orbital model is that one of the "t_{2g}" levels is not purely involved in π type interactions but has mixed with one of the "e_g" orbitals of the same symmetry. We have shown this on the diagram and labeled the stabilization with the letter P. This interaction is quite large and actually influences the energetics of distortion considerably. Figure 31 shows the energy difference curve between distortions of types A and B as a function of d count taking into account this mixing. It is very similar indeed to that computed by using a full band structure calculation on the full three-dimensional solid, Figure 29. From a comparison of Figure 28 and Figure 30, we can see that there is an interesting competition

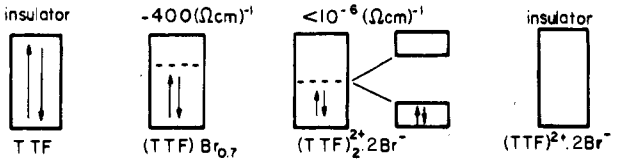

Figure 32. Electronic and structural behavior of TTF. (Reprinted with permission from ref 1a. Copyright 1984 Pergamon Press.)

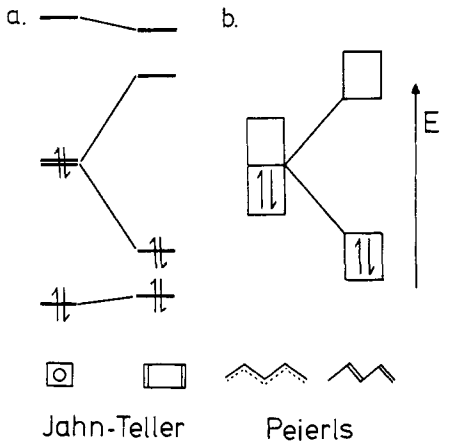

Figure 33. Similarity between Jahn–Teller and Peierls distortions.

between the geometrical preferences of the local coordination geometry and that of the orbital mixing induced by the presence of the infinite chain. Similar results are found for two-dimensional sheet structures containing linked octahedra, such as the cadmium halide type.[107] Notice that although molecular orbital arguments enable us to handle this problem, the crystal field approach does not.

E. Peierls Distortions and Structure

One area that has seen increasing interest by the chemical community in recent years has been the study of low-dimensional materials. These are systems which are often built up from molecules which in their pristine condition would be insulators or semiconductors. On doping with either donors or (more usually) acceptors these materials become metallic. This is shown schematically in Figure 32 for the species TTF.[85] As electron density is removed from the energy band the system changes from being a semiconductor to being a metal. Notice however that the system with a half-filled band is an insulator too. This comes about in an interesting way. Just as a half-filled pair of degenerate molecular orbitals leads to a structural (Jahn–Teller) distortion in molecules, so a half-filled band in a one-dimensional material is subject to a similar (Peierls) instability. The best way of showing this is to consider a one-dimensional chain of $p\pi$ orbitals. This would occur for the polymer $(CH)_x$–polyacetylene. With one pi electron per atom this energy band would be half full. Figure 33 shows the analogy between cyclobutadiene and polyacetylene. Both are half-filled orbital problems. Notice that within the Hückel formalism the π band width and other details are quantitatively similar in the two. Cyclobutadiene does not have a square geometry, but whether it has a rectangular or rhomboid structure is not yet clear. Polyacetylene has a bond alternating pattern, the Peierls distorted arrangement.

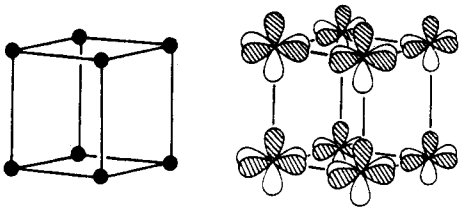

Figure 34. The simple cubic structure and the orthogonal p orbitals at each site. (Reprinted with permission from ref 109. Copyright 1983 The American Chemical Society.)

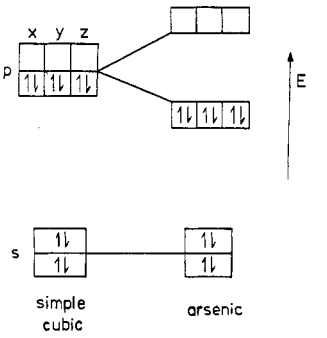

Figure 35. Schematic band structure picture for the distortion of the simple cubic structure to that of arsenic. (Reprinted with permission from ref 109. Copyright 1983 The American Chemical Society.)

One of the challenges facing the chemist in this area is the determination of the extent of bond alternation. It has not proven possible to make good single crsytals of polyacetylene in order to determine this number accurately.

Substitution patterns of square cyclobutadiene were mentioned in section IVB. There we were interested in seeing which of two patterns was more stable. However there is an important comment to be made concerning the stability of the substituted structure relative to the parent. By the alternate substitution of either the carbon atoms themselves or the groups attached to them, by atoms of disparate electronegativity, the regular square structure may be stabilized.[108] Indeed as we have noted above there are several known examples. It is then an intriguing possibility, given the isomorphism of Figure 33, to design a substituted polyacetylene which would have equal bond lengths.

There are other more complex structures which are understandable[109] using the structural consequences of the Peierls concept. Consider the simple cubic structure shown in Figure 34, where each site is populated with an atom with valence s and p orbitals. Let us assume for simplicity that the s orbital may be ignored except as a storage location for two electrons and that the salient features of the electronic problem may be handled by consideration of the valence p orbital manifold. If we ignore π-type overlap between the p orbitals on adjacent atoms, then the result is an extremely simple electronic problem, that of three mutually orthogonal one-dimensional p bands. For a group 15 element, with an atomic configuration s^2p^3 the s band will be full and we may envisage each of the three p bands to be exactly half full. With this electronic configuration the simple cubic structure should then distort by breaking each alternate linkage in each of the three directions as a result of the electronic situation shown in Figure 35. The number of possibilities in general is enormous,[110] but the structures of elemental arsenic and black

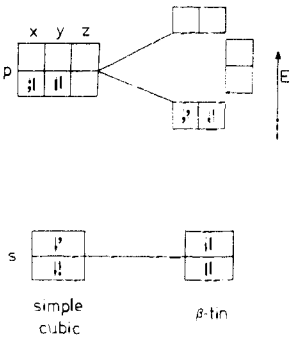

Figure 36. Schematic band structure for the distortion of the simple cubic structure to that of β-tin. (Reprinted with permission from ref 109. Copyright 1983 The American Chemical Society.)

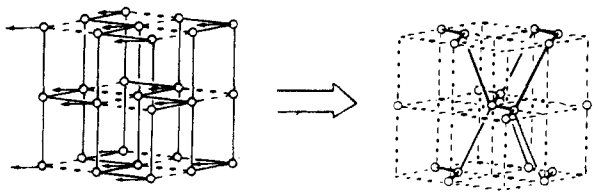

Figure 37. Generation of the β-tin structure. (Reprinted with permission from ref 109. Copyright 1983 The American Chemical Society.)

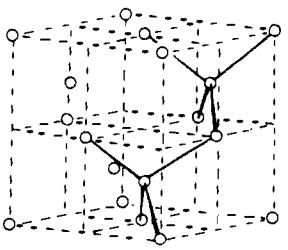

Figure 38. The diamond structure. (Reprinted with permission from ref 109. Copyright 1983 The American Chemical Society.)

phosphorus which have small unit cells are readily derived in this way. **30** shows the process in an idealized fashion. The actual structures are those which have relaxed from the simple picture so that the bonded and nonbonded distances are different. For small cells the number of structural possibilities achievable by this route is not too large. For example there are only 36 different ways of breaking up the simple cubic structure to give arrangements with trigonal-pyramidal coordination at each site, if we start off with a cell the size of the one in **30**. Elsewhere[111] we discuss the factors which differentially stabilize these alternatives. Note that the arsenic structure may be derived from several different viewpoints, including those of Scheme II and that presented here in terms of the Peierls approach.

We can view the structures of the AB octet compounds in this way. These compounds, with an average of four electrons per atom, were discussed in section IIIB. There we examined the models used to predict whether the six-coordinate rock salt structure (a derivative of the simple cubic structure) or four-coordinate sphalerite structure (a derivative of cubic diamond) was observed. Figure 36 shows the electronic situation for systems with the s^2p^2 configuration. There are now only two half-filled bands, and the structure should distort to an arrangement where half the linkages are broken along two directions only. One way of doing this is shown in Figure 37. This leads to the β-tin structure, one which is closely related to diamond, Figure 38.

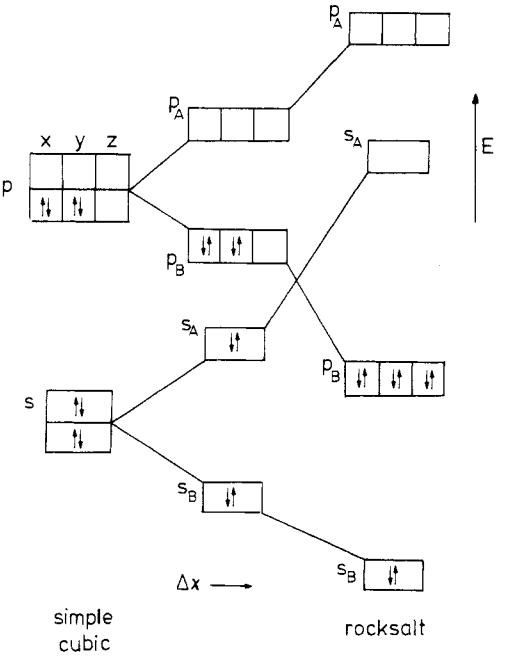

Figure 39. Schematic band structure picture for the distortion of the simple cubic structure to that of rocksalt. (Reprinted with permission from ref 109. Copyright 1983 The American Chemical Society.)

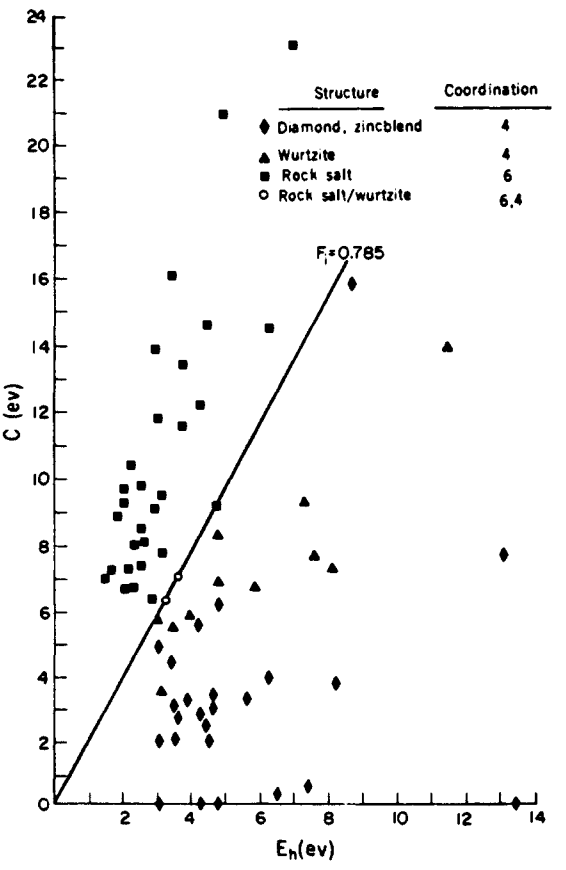

Figure 40. Structure map using the Phillips–van Vechten indices. (Reprinted with permission from ref 112. Copyright 1973 Plenum Press.)

Figure 39 shows how the energy bands of such a simple cubic arrangement change in energy as the electronegativity difference ($\Delta\chi$) between A and B is increased. It is interesting to see how the Peierls instability is removed. We expect therefore to see an increase in the stability of the simple cubic derivative (rock salt) as $\Delta\chi$

increases. This is actually found in practice. Figure 40 shows a structure map[112] using as indices parameters from the electronegativity scheme of Phillips and Van Vechten, which perfectly sorts all known octet structures. There is a critical value of the ionicity at which the crossover occurs. This result has been reproduced theoretically via pseudopotential-based band structure calculations.[113]

Acknowledgments. This research has been supported by the National Science Foundation under grants NSF DMR8414175 and DMR8216892, by the Donors of The Petroleum Research Fund, administered by The American Chemical Society, and by the Dow Chemical Company. I would like to thank Stephen Lee and Gordon Miller, many of whose ideas appear in this article. I have also benefitted from several useful conversations with F. C. Hawthorne, B. G. Hyde, P. B. Moore, M. O'Keeffe and J. V. Smith. I acknowledge permission for the following reproductions: Academic Press for **13**, The Mineralogical Society of America for **27**, Springer-Verlag for **23–26**, P. B. Moore for **10**, MacMillan Journals for **7**, Butterworth for **9**, and The American Chemical Society for **3–5**, 11, **12**, **14–22**, **30**, **32–36**.

References

(1) See, for example: Burdett, J. K. *Prog. Solid State Chem.* **1984**, *15*, 173. Whangbo, M.-H. In *Crystal Chemistry and Properties of Materials with Quasi-One*-Dimensional Structures; Rouxel, J., Ed.; Reidel: Dordrecht, 1986. Hoffmann, R. *Angew. Chem.*, in press.
(2) See the collection of papers in: *The Structures of Complex Solids*; Navrotsky, A., O'Keeffe, M., Eds.; Academic: New York, 1981.
(3) Roberts, P. J.; Ferguson, G. *Acta Crystallogr., Sect. B: Struct. Cryst. Chem.* **1977**, *B33*, 2335.
(4) Chiang, M. Y.; Böhlen, E.; Bau, R. *J. Am. Chem. Soc.* **1985**, *107*, 1679.
(5) Massa, H.; Kujanek, R.; Baum, S.; Dehnicke, K. *Angew. Chem., Int. Ed. Engl.* **1984**, *23*, 149.
(6) There is a superb series of volumes (1–10, 1974–1982) published by the American Mineralogical Society entitled *Reviews in Mineralogy*; Ribbe, P. H., Ed.
(7) Smith, J. V. *Feldspar Minerals, I. Crystal Structure and Physical Properties*; Springer-Verlag: Berlin, 1974.
(8) Moore, P. B.; Sen Gupta, P. K.; Schlemper, E. O. *Nature (London)* **1985**, *318*, 548.
(9) McConnell, J. D. C. *Am. Mineral.* **1983**, *68*, 1.
(10) See the discussion and references in: Cheetham, A. K.; Fyfe, C. A.; Smith, J. V.; Thomas, J. M. *J. Chem. Soc., Chem. Commun.* **1982**, 823.
(11) Pluth, J. J.; Smith, J. V.; Kvick, Å. *Zeolites* **1985**, *5*, 74.
(12) Smith, J. V. *Chem. Rev.* **1988**, *88*, 149.
(13) Moore, P. B. *Nature (London)* **1983**, *306*, 5491.
(14) See: Seff, K.; Mellum, M. D. *J. Phys. Chem.* **1984**, *88*, 3560 and the complete set of references therein.
(15) Huheey, J. E. *Inorganic Chemistry*, 2nd ed.; Harper and Row: New York, 1978.
(16) Pluth, J. J.; Smith, J. V. *J. Phys. Chem.* **1979**, *83*, 741.
(17) Pluth, J. J.; Smith, J. V. *J. Am. Chem. Soc.* **1983**, *105*, 1192.
(18) Fitch, A. N.; Jobic, H.; Renouprez, A. *J. Phys. Chem.* **1986**, *90*, 1311.
(19) Yanagida, R. Y.; Vance, T. B.; Seff, K. *Inorg. Chem.* **1974**, *13*, 723.
(20) Gibbs, G. V. *Am. Mineral.* **1982**, *67*, 421. Geisinger, K. L.; Gibbs, G. V. *Phys. Chem. Miner.* **1981**, *7*, 204.
(21) Gibbs, G. V.; Meagher, E. P.; Newton, M. D.; Swanson, D. K. In Reference 2.
(22) O'Keeffe, M.; Hyde, B. G. *J. Solid State Chem.* **1982**, *44*, 24.
(23) O'Keeffe, M.; Hyde, B. G. In Reference 2.
(24) Da Silva, J. R. G.; Pinatti, D. G.; Anderson, C. E.; Rudee, M. L. *Philos. Mag.* **1975**, *31*, 713.
(25) Albright, T. A.; Burdett, J. K.; Whangbo, M.-H. *Orbital Interactions in Chemistry*; Wiley: New York, 1985.
(26) Burdett, J. K.; Hughbanks, T.; Miller, G. J.; Richardson, J. W.; Smith, J. V. *J. Am. Chem. Soc.* **1987**, *109*, 3639.
(27) Smith, W. H.; Barrett, J. J. *J. Chem. Phys.* **1969**, *51*, 1475.
(28) Winter, J. K.; Ghose, S.; Okamura, F. P. *Am. Mineral.* **1977**, *62*, 921.
(29) Smith, J. V.; Pluth, J. J.; Faber, J. *J. Appl. Phys.* **1985**, *57*, 1045.
(30) Hazen, R. M.; Finger, L. W. *Comparative Crystal Chemistry*; Wiley: New York, 1982.
(31) Hazen, R. M.; Finger, L. W. *Am. Sci.* **1984**, April.
(32) Newton, M. D. In Reference 2.
(33) Weiss, V. A.; Weiss, A. *Z. Anorg. Allg. Chem.* **1984**, *276*, 95.
(34) Grey, I. E. *J. Solid State Chem.* **1974**, *11*, 128.
(35) O'Keeffe, M.; Gibbs, G. V. *J. Chem. Phys.* **1984**, *81*, 876.
(36) Fink, M. J.; Haller, K. J.; West, R.; Michl, J. *J. Am. Chem. Soc.* **1984**, *106*, 822.
(37) Power, P., personal communication.
(38) Edge, R. A.; Taylor, H. F. W. *Nature (London)* **1969**, *224*, 304.
(39) Moore, P. B.; Araki, T. *Neues. Jahrb. Mineral. Abh.* **1978**, *132*, 231.
(40) Clark, G. M. *The Structures of Non-Molecular Solids*; Applied Science: London, 1972.
(41) O'Keeffe, M. *Acta Crystallogr., Sect. A: Cryst. Phys., Diffr., Theor. Gen. Crystallogr.* **1977**, *A33*, 924.
(42) McLarnan, T. J. *Z. Kristallogr.* **1981**, *155*, 227, 247, 269.
(43) Mitchell, R. S. *Z. Kristallogr.* **1956**, *108*, 296.
(44) Andersson, S.; Hyde, S. T.; von Schnering, H. G. *Z. Kristallogr.* **1984**, *168*, 1. Hyde, S. T.; Andersson, S.; Ericsson, B.; Larsson, K. *Z. Kristallogr.* **1984**, *168*, 213.
(45) Wykoff, R. G. W. *Crystal Structures*; Wiley: New York, 1951.
(46) O'Keeffe, M.; Hyde, B. G. *Struct. Bonding (Berlin)* **1985**, *61*, 77.
(47) Moore, P. B., to be submitted for publication.
(48) Moore, P. B. *Neues Jahrb. Mineral., Abh.* **1976**, *127*, 187.
(49) Araki, T.; Moore, P. B. *Am. Mineral.* **1981**, *66*, 827.
(50) Pauling, L. *J. Am. Chem. Soc.* **1929**, *51*, 1010.
(51) Allmann, R. *Monatsh. Chem.* **1975**, *106*, 779.
(52) Brown, I. D. *Acta Crystallogr., Sect. B: Struct. Crystallogr. Cryst. Chem.* **1977**, *B33*, 1305.
(53) Brown, I. D.; Altermatt, D. *Acta Crystallogr., Sect. B: Struct. Sci.* **1985**, *B41*, 244.
(54) Baur, W. H.; McLarnan, T. J. *J. Solid State Chem.* **1982**, *42*, 300. McLarnan, T. J.; Baur; W. H. *J. Solid State Chem.* **1982**, *42*, 283.
(55) Baur, W. H. *Trans. Am. Cryst. Assoc.* **1970**, *6*, 129.
(56) Altermatt, D.; Brown, I. D. *Acta Crystallogr., Sect. B: Struct. Sci.* **1985**, *B41*, 244.
(57) Burdett, J. K.; Hawthorne; F. C., to be submitted for publication.
(58) Burdett, J. K. *Molecular Shapes*; Wiley: New York, 1980.
(59) McCarley, R. E.; Li, K.-H.; Edwarts, P. A.; Brough, L. F. *J. Solid State Chem.* **1985**, *57*, 17.
(60) Brown, I. D. In Reference 2.
(61) Brown, I. D. *Phys. Chem. Miner.*, in press.
(62) Garrett, J. D.; Greedan, J. E.; Faggiani, R.; Carbotte, S.; Brown, I. D. *J. Solid State Chem.* **1982**, *42*, 183.
(63) Pauling, L. *The Nature of the Chemical Bond*, 3rd ed.; Cornell University: Ithaca, NY, 1960.
(64) Shannon, R. D. *Acta Crystallogr., Sect. A: Cryst. Phys. Diffr. Theor. Gen. Crystallogr.* **1976**, *A32*, 751.
(65) Shannon, R. D. in Reference 2.
(66) O'Keeffe, M. In Reference 2.
(67) Johnson, D. A. *Some Thermodynamic Aspects of Inorganic Chemistry*; Cambridge University: New York, 1968.
(68) Burdett, J. K.; Smyth, J., to be submitted for publication.
(69) Allinger, N. L.; Tribble, M. T.; Miller, M. A.; Wertz, D. H. *J. Am. Chem. Soc.* **1971**, *93*, 1037.
(70) Catlow, C. R. A. *Annu. Rev. Mater. Sci.* **1986**, *16*, 517.
(71) Gibbs, G. V.; Lasaga, A. *Phys. Chem. Miner.* **1987**, *14*, 107.
(72) (a) St. John, J.; Bloch, A. N. *Phys. Rev. Lett.* **1974**, *33*, 1095. (b) Zunger, A. *Phys. Rev. B: Condens. Matter* **1980**, *22*, 5839.
(73) Chelikowsky, J. R.; Phillips, J. C. *Phys. Rev. B: Condens. Matter* **1978**, *17*, 2453.
(74) Burdett, J. K.; Price, G. D.; Price, S. L. *Phys. Rev. B: Condens. Matter* **1981**, *24*, 2903.
(75) Cohen, M. L. in ref 2; *Phys. Today* **1979**, *32*, 40.
(76) Yin, M. T.; Cohen, M. L. *Phys. Rev. Lett.* **1980**, *45*, 1004.
(77) Burdett, J. K.; Price, G. D.; Price, S. L. *J. Am. Chem. Soc.* **1982**, *104*, 92.
(78) Price, G. D.; Price, S. L.; Burdett, J. K. *Phys. Chem. Miner.* **1982**, *8*, 69.
(79) Bürgi, H.-B. *Angew. Chem., Int. Ed. Engl.* **1975**, *14*, 460.
(80) Murray-Rust, P.; Bürgi, H.-B.; Dunitz, J. D. *J. Am. Chem. Soc.* **1975**, *97*, 921.
(81) Burdett, J. K. *Inorg. Chem.* **1979**, *18*, 1024.
(82) Murray-Rust, P., unpublished data.
(83) Burdett, J. K. *Inorg. Chem.* **1975**, *14*, 931; **1977**, *16*, 3013.
(84) Forbus, T. R.; Martin, J. C. *J. Am. Chem. Soc.* **1979**, *101*, 5057.
(85) Ashcroft, N. W.; Mermin, N. D. *Solid State Physics*; W. B. Saunders: Philadelphia, 1976.
(86) Mingos, D. M. P. *Nature (London), Phys. Sci.* **1972**, *236*, 99.

(87) Burdett, J. K. *Nature (London)* **1979**, *279*, 121.
(88) Jeitschko, W. *Acta Crsytallogr., Sect. B: Struct. Crystallogr. Cryst. Chem.* **1974**, *B30*, 2565.
(89) Burdett, J. K.; Canadell, E.; Miller, G. J. *J. Am. Chem. Soc.* **1986**, *108*, 6561.
(90) Dixon, D. E.; Parry, G. S. *J. Phys. C* **1962**, *C2* 1732.
(91) Burdett, J. K.; Lee, S.; McLarnan, T. J. *J. Am. Chem. Soc.* **1985**, *107*, 3083.
(92) Burdett, J. K.; Lee, S. *J. Am. Chem. Soc.* **1985**, *107*, 3050.
(93) Burdett, J. K. *Struct. Bonding (Berlin)* **1987**, *65*, 30.
(94) Burdett, J. K.; McLarnan, T. J. *J. Solid State Chem.* **1984**, *53*, 382.
(95) Burdett, J. K.; Canadell, E.; Hughbanks, T. *J. Am. Chem. Soc.* **1986**, *108*, 3971.
(96) Bauer, J.; Bars, I. *Acta Crystallogr., Sect. B: Struct. Crystallogr. Cryst. Chem.* **1980**, *B36*, 1540.
(97) Weiger, G. A.; Jellinek, F. *J. Solid State Chem.* **1970**, *1*, 519.
(98) Burdett, J. K. *Inorg. Chem.* **1985**, *24*, 2244.
(99) Krogh-Jesperson, K.; Cremer, D.; Poppinger, D.; Pople, J. A.; Schleyer, P. v. R.; Chandresekhar, J. *J. Am. Chem. Soc.* **1979**, *101*, 4843.
(100) Burdett, J. K.; Hughbanks, T. *J. Am. Chem. Soc.* **1984**, *106*, 3101.
(101) See for example: Wells, A. F. *Structural Inorganic Chemistry*, 5th ed.; Oxford University: London, 1984.
(102) Kirby, A. J. *The Anomeric Effect and Related Stereoelectronic Effects at Oxygen*; Springer-Verlag: Berlin, 1983.
(103) Hout, R. F.; Pietro, W. J.; Hehre, W. J. *An Approach to Molecular Structure and Reactivity*; Wiley: New York, 1984.
(104) Smyth, J. R.; Smith, J. V.; Artioli, G.; Kvick, Å. *J. Phys. Chem.* **1987**, *91*, 988.
(105) Burdett, J. K. *Inorg. Chem.* **1981**, *20*, 1959.
(106) Burdett, J. K.; Miller, G. J.; Richardson, J. W.; Smith, J. V., to be submitted for publication.
(107) Burdett, J. K.; Kulkarni, G. V., to be submitted for publication.
(108) Hoffmann, R. *J. Chem. Soc., Chem. Commun.* **1979**, *240*.
(109) Burdett, J. K.; Lee, S. *J. Am. Chem. Soc.* **1983**, *105*, 1079.
(110) Burdett, J. K.; McLarnan, T. J. *J. Chem. Phys.* **1981**, *75*, 5764.
(111) Burdett, J. K.; McLarnan, T. J. *J. Chem. Phys.* **1981**, *75*, 5774.
(112) Phillips, J. C. In *Treatise on Solid State Chemistry*; Hannay, N. B., Ed.; Plenum: New York, 1973; Vol. 4.
(113) Chelikowsky, J. R.; Burdett, J. K. *Phys. Rev. Lett.* **1986**, *56*, 961.